รายงานวิจัยฉบับสมบูรณ์

การพัฒนาตัวเร่งปฏิกิริยาโลหะเหล็กที่มีประสิทธิภาพสำหรับการย่อยสลายสารอินทรีย์ในน้ำ

โดย

ดร. การะเกด เทศศรี

มิถุนายน 2558

สัญญาเลขที่ MRG 5680158

รายงานวิจัยฉบับสมบูรณ์

การพัฒนาตัวเร่งปฏิกิริยาโลหะเหล็กที่มีประสิทธิภาพสำหรับการย่อยสลายสารอินทรีย์ในน้ำ

.....

ดร. การะเกด เทศศรี มหาวิทยาลัยบูรพา

สนับสนุนโดยสำนักงานกองทุนสนับสนุนการวิจัย

(ความเห็นในรายงานนี้เป็นของผู้วิจัย สกว.ไม่จำเป็นต้องเห็นด้วยเสมอไป)

รหัสโครงการ : MRG 5680158

ชื่อโครงการ: การพัฒนาตัวเร่งปฏิกิริยาโลหะเหล็กที่มีประสิทธิภาพสำหรับการย่อยสลายสารอินทรีย์ในน้ำ

ชื่อนักวิจัยและสถาบัน : ดร. การะเกด เทศศรี มหาวิทยาลัยบูรพา

E-mail Address : karaked@buu.ac.th

ระยะเวลาโครงการ: 2 ปี

บทคัดย่อ

อนุภาคนาโนโลหะเหล็กได้รับการยอมรับว่ามีประสิทธิภาพสูงในการย่อยสลายสารปนเปื้อนอินทรีย์ที่มีหมู่คลอโรเป็นองค์ประกอบได้หลากหลายชนิด แต่เป็นที่ทราบว่าไม่มีประสิทธิภาพในการย่อยสลาย 1,2 ไดคลอโรอีเทนได้อย่างมีนัยสำคัญ งานวิจัยนี้แสดงให้เห็นเป็นครั้งแรกว่า อนุภาคนาโนโลหะคู่แพลเลเดียม/เหล็กที่มีเซลลูโลสเป็นสารช่วยเสถียร (Pd/CMC-Fe^0 nanoparticles) มีประสิทธิภาพในการย่อยสลาย 1,2 ไดคลอโรอีเทนได้สูงถึงร้อยละ 14 อนุภาคนาโนโลหะเหล็กสามารถสังเคราะห์ได้ภายใต้สภาวะที่มีสารช่วยเสถียรที่แตกต่างกัน ได้แก่ เซลลูโลส (CMC) และแป้ง และวัสดุรองรับที่แตกต่างกัน ได้แก่ อนุภาคนาโนซิกาที่มีรูพรุนระดับมีโซ และถ่านกัมมันต์ เพื่อป้องกันการรวมตัวของอนุภาค การควบคุมการสังเคราะห์ที่สภาวะต่างๆ ทำให้ได้อนุภาคนาโนโลหะเหล็กที่มีขนาดต่างๆ ในช่วง 12-75 นาโนเมตร อนุภาคนาโนโลหะคู่แพลเลเดียม/เหล็ก เตรียมได้จากการผสมกันระหว่างอนุภาคนาโนโลหะเหล็กและแพลเลเดียมในรูปคอลลอยด์ก่อนนำมาใช้เป็นตัวเร่งปฏิกิริยา วิเคราะห์ขนาดอนุภาค สัณฐาน โครงสร้างพื้นผิว และองค์ประกอบพื้นผิวของตัวอย่างที่สังเคราะห์ได้โดยเทคนิคต่างๆ ติดตามความเสถียรของการกระจายตัวในรูปคอลลอยด์และการเคลื่อนที่ของอนุภาค นอกจากนี้ศึกษาประสิทธิภาพในการกำจัด 1,2 ไดคลอโรอีเทน ที่ปนเปื้อนในแหล่งน้ำใต้ดินบริเวณ 3 ชุมชนใกล้เคียงนิคมอุตสาหกรรมมาบตาพุดเพื่อใช้เป็นกรณีศึกษา

คำหลัก : การกำจัดหมู่คลอโร, 1,2 ไดคลอโรอีเทน, อนุภาคนาโนโลหะเหล็ก, อนุภาคนาโนโลหะคู่

Project Code : MRG 5680158

Project Title : Development of Active Iron-based Nanoparticles for the Degradation of Toxic Contaminants in Water

Investigator : Dr. Karaked Tedsree, Burapha University

E-mail Address : karaked@buu.ac.th

Project Period : 2 years

Abstract

Zero-valent iron nanoparticle was accepted as a high performance material to degrade a wide variety of chlorinated contaminants, however its catalytic activity towards 1,2-dichloroethane has been known insignificant. This work, it is demonstrate for the first time that 1,2-dichloroethane was significant degraded up to 14% by Pd modified CMC stabilized Fe^0 bimetallic nanoparticles (Pd/CMC-Fe^0 nanoparticles). Zero-valent iron nanoparticles (Fe^0 nanoparticles) were synthesized in the presence of different types of stabilizers (CMC and soluble starch) and support materials (mesoporous silica and activated carbon) to prevent nanoparticles from aggregation. Discreate Fe^0 nanoparticles with the particle size in range 12-75 nm were obtained by control synthesis at different conditions. Pd/CMC-Fe^0 nanoparticles were prepared by mixing colloidal suspension of Fe nanoparticles and Pd nanoparticles before using as a catalyst. Particle size, morphology crystal structure and surface structure of all synthesized samples were characterized by various techniques. Dispersion stability and particle mobility of the synthesized Fe^0 naoparticles were also monitored. In addition, a case study of the dechlorination efficiency of contaminants groundwater collected from 3 communities nearby Map Ta Phut industrial estate was also investigated.

Keywords : Dechlorination, 1,2 dichloroethane, zero-valent iron nanoparticle, bimetallic nanoparticle

CHAPTER 1
INTRODUCTION

Chlorinated organic compounds (COCs) are widespread environmental contaminants found both in groundwater and soil, many of which are toxic, persistent and poorly biodegradable to biota. They can accumulate gradually in the environment and turn to be a threat to human and ecosystem long-standing. The remediation of groundwater and soil contaminated by COCs has an extensive concern and is becoming a significant priority (Wang et al., 2009).

Since the late 1990s, the use of zero valent iron for groundwater remediation has been investigated for its potential to reduce subsurface contaminants such as chlorinated solvents and heavy metal. Currently, nanoscale zero valent iron particles shows tremendous promise in the environmental sector due to its high reactivity. With a large surface-to-volume ratio of nanoscale materials, zero-valent iron nanoparticles can effectively oxidize many robust toxic contaminants in a short time (Li et al., 2006). In addition, the degradation can work well in both acid and base conditions. The aggregative toxic compounds such chlorinated hydrocarbon can be either decomposed or transformed to non-toxic forms by the iron nanoparticles. Moreover, the catalytic performance of iron nanoparticles can be significantly improved by blending with a small quantity of additives/promoters or with the use cost-effective high performance support materials. Therefore, the employment of nanoscale zero-valent iron nanoparticles in environment remediation is a promising technology which may solve some challenge problems in water cleanup facing Thailand.

In addition to reactivity, the stability of nanoscale iron particles is also of a major concern. Nanoscale iron particles exhibit high van der Waal attractions also have high magnetic properties which cause the particles to agglomerate are not stable in suspensions for long period of time (Cirtiu et al., 2011). The sedimentation and agglomeration of nanoscale iron particles impede the delivery of nanoscale iron particles into the contaminated zones during the in-situ applications. Thus, the preparation of zero-valent iron nanoparticles with high dispersion stability and high mobility is still challenge.

Researchers have been trying to modify the surface of the nanoscale iron particles to make them more stable in suspension and ensure adequate reactivity as well as mobility to deliver into the contaminated subsurface zones (Richard L. et al., 2009). A wide variety of stabilizers have been proposed to modify zero-valent iron nanoparticle surface characteristics. In addition, increasing efforts have been directed on the dispersion of iron nanoparticles on support materials which can effectively protect iron core from being oxidized (Petala et al., 2013). Simultaneously, one should consider that modified nanoscale iron nanoparticles should be able to transport through the soils while maintaining adequate reactivity with the target contaminants under subsurface conditions.

1,2-Dichloroethane is a raw material used for the manufacture of vinyl chloride monomer (VCM) and therefore has very often been detected in the groundwater nearby the VCM manufacturing plant (Huang et al., 2011). It is one of the most stable chlorinated hydrocarbons with categorized as a very recalcitrant groundwater contaminant. Although, zero-valent iron is capable of degrading a wide array of highly chlorinated contaminants such as trichloroethylene, vinyl chloride, carbon tetrachloride, and tetrachloroethane, its catalytic activity towards 1,2-dichloroethane is insignificant. Thus**,** 1,2-dichloroethane remains a challenging compound for the remediation community and one of the great research interests.

For this proposed research, development of high performance surface modified iron nanoparticles to treat 1,2- dichloroethane (DCA) contaminated in groundwater will be focused. The experiments will first be carried out in laboratory scale by using standardized water but at later stage, contaminated water samples from the community nearby Map Ta Phut industrial estate will be studied such that various factors can be identified to meet high activity, stability and mobility under the limited conditions of cost effective and environmentally friendly iron nanoparticles,

For the development of high performance zero-valent iron nanoparticles, the preparation of iron nanoparticles will be focused on

1. High surface to volume ratio of active sites
2. High stability; stable in air and remain in suspensions for long period of time
3. High mobility, high ability to pass through porous media.

Objectives

1. To synthesize zero-valent iron nanoparticles as high performance (reactivity, stability and mobility) catalysts fordechlorination of 1,2 dichloroethane contaminate in groundwater.
2. To systematically study the important parameters such as catalyst formulation, composition and structures as well as reaction conditions that affect to the dechlorination efficiency.
3. To study the contaminated water samples from the community nearby Map Ta Phut industrial estate such that various factors can be identified and treated.

CHAPTER 2

RESEARCH METHODOLOGY

The experiments were carried out in an aqueous solution under N_2 atmosphere. Deionized water was purged with N_2 gas to removed dissolved oxygen. Bare and coated zero-valent iron nanoparticles were prepared. In addition, zero-valent iron nanoparticles on mesoporous silica and carbon material support were prepared.

Section I: Synthesis of Zero-valent Iron Nanoparticles

2.1 Synthesis of Bare Zero-valent Iron Nanoparticles

Bare iron nanoparticles were prepared by mixing an equal volume of an aqueous solution of 2.0 M $NaBH_4$ and 0.01M $FeCl_3$. The sodium borohydride solution was slowly added into the iron chloride solution under N_2 atmosphere and stirred for 2h. The colour of solution will be changed slowly from yellow to black. The obtained iron nanoparticles were separated from the mixture by centrifugation, washed several times with deionized water and ethanol before used or stored in dry methanol.

2.2 Synthesis of Polymer-Stabilized Zero-valent Iron Nanoparticles

Sodium carboxy methyl cellulose (Na-CMC) and water soluble starch were used as green-polymer stabilizer to protect Fe^0 nanoparticles from aggregration.

2.2.1 Synthesis of CMC-Stabilized Zero-valent Iron Nanoparticles (CMC-Fe^0 Nanoparticles)

In the typical experiment, CMC 2.5 g was dissolved in 100 mL of water. $FeCl_3$ 0.162g was dissolved in 100 ml of water (ratio CMC-Fe^{3+} is 10:1). The above prepared solution was mixed and stirred at room temperature. 5% NH_4OH solution was slowly dropped to keep the solution at pH ≈ 8. Approximately 20 mL of 4.0M an aqueous $NaBH_4$ solution was added dropwise under N_2 atmosphere and stirred for desired time. The colour of solution will be changed slowly from yellow to black. The obtained iron nanoparticles were separated from the mixture by centrifugation, washed several times with deionized water and ethanol before used or stored in dry methanol.

The effect of reaction temperature, reaction time, concentration of Fe^{3+} precursor and ratio of Fe to CMC stabilizer was studied. Reaction temperature was study at room temperature and 60°C. Mole ratio of Fe precursor to CMC (monomer) was studied at 1:5 and 1:10 (CMC). Concentration of Fe^{3+} precursor was studied at 0.01 M and 0.02 M. Reaction time was studied between 4-48 h.

2.2.2 Synthesis of Starch-stabilized Zero-valent Iron Nanoparticles (STR-Fe^0) Nanoparticles)

The same preparation method of CMC-Fe^0 nanoparticles was applied to prepare starch-stabilized colloidal Fe^0 nanoparticles. However, the amount of $FeCl_3$ was 0.162g and water soluble starch was 1.620 g dissolved in 100 ml of water at 60◦C (ratio starch-Fe^{3+} is 10:1). The above prepared solution was mixed and stirred at room temperature. 5% NH_4OH solution was slowly dropped to keep the solution at pH ≈ 8. The mixture was stirred at room temperature. 20 mL of 4.0M $NaBH_4$ aqueous solution was added dropwise under N_2 atmosphere and stirred in oil bath at 60◦C for 2h. The color of solution will be changed slowly from yellow to black. The obtained iron nanoparticles were separated from the mixture by centrifugation, washed several times with deionized water and ethanol before used or stored in dry methanol.

2.3 Synthesis of Zero-valent Iron Nanoparticles on Material Supports

2.3.1 Synthesis of Mesoporous Silica Nanoparticles

0.5g of CTAB was dissolved in 240 mL of deionized water. 1.75 mL of an aqueous solution of 2M NaOH was added into the solution. The temperature was adjusted to 80°C and 2.5 mL of TEOs was added dropwise to the flask under stirring. The reaction was continued heating for 2h at 80°C. The resulting white precipitate was filtered, washed with water and ethanol, dried at 100°C for 4h and calcined for 4h at 600°C.

2.3.2 Synthesis of Zero-valent Iron Nanoparticles supported on Mesoporous Silica Nanoparticles (Fe^0/SiO_2 Nanoprticles)

Mesoporous support zero-valent iron nanoprticles was prepared by wet impregnation. In typical experiment, 0.6 g of prepared mesoporous silica was dispersed in

30 ml of 0.01 M $FeCl_3$. The suspension was heated at 60°C to evaporate water until nearly dry. 20 ml of water was added and filtration. 50 ml of water was added in Fe^{3+}/SiO_2 and sonicate. Then, 20 mL of 4.0M $NaBH_4$ aqueous solution was added dropwise under N_2 atmosphere and stirred stirred for 4 hr. The obtained mesoporous silica support zero-valent iron nanoprticles were separated from the mixture by centrifugation, washed several times with deionized water and ethanol before use or stored in dry methanol.

2.3.3 Synthesis of Zero-valent Iron Nanoparticles on Activated Carbon Supporting (Fe^0/C Nanoparticles)

Pretreatment of Activated Carbon: Activated Carbon as support was pretreated before using. 1.00 g of activated carbon was refluxed in 200 mL of 35% HNO_3 for 2 h. The obtained pretreated carbon was then centrifugation, washed with water until water washing is neutral pH and dried at 100°C for 6h.

2.3.4 Carbon support Zero-valent Iron Nanoprticles (Fe^0/C)

0.6 g of pretreated carbon was dispersed in 50 ml 0.01M $FeCl_3$ (10% Fe on carbon support). The suspension was mixed and stirred at room temperature. 5% NH_4OH solution was slowly dropped to keep the solution at pH ≈ 8. 20 mL of 4.0 M $NaBH_4$ aqueous solution was added dropwise under N_2 atmosphere and stirred for 4h. The obtained iron nanoparticles were separated from the mixture by centrifugation, washed several times with deionized water and ethanol before use or stored in dry methanol.

2.4 Synthesis of Pd-Modified CMC-stabilized Iron Nanoparticle (Pd/CMC-Fe^0 Nanoparticles).

Pd modified Iron nanoparticles were prepared by palladization and nano-palladium deposition method.

2.4.1 Palladization Method

0.028g of $Pd(NO_3)_2$ in 15 ml of water was added in the colloidal iron nanoparticles suspension prepared from 3.3.2 section. The mixture was stirred at room temperature for 1 h. The obtained iron Pd/Fe nanoparticles were separated from the mixture by centrifugation, washed several times with deionized water and ethanol before use or stored in dry methanol. Various ratios of Pd loading were prepared at 0.1, 0.2, 0.3, and 0.5 % loading.

2.4.2 Nano-palladium Deposition

Pd-Modified CMC-stabilized iron nanoparticles were prepared in 2 steps. CMC-Fe nanoparticles and Pd nanoparticles were separately prepared and chemically mixing in colloidal form.

Preparation of Pd Colloidal Nanoparticles

In a 100 mL round bottom flask, 0.0280g of $Pd(NO_3)_2$ and 0.24 g (2.1628×10^{-3} moles) of PVP were dissolved in 15 mL of diethylene polyol under stirring. The solution was then heated at 90°C. After 2 h at 90 °C, a transparent dark brown colloidal solution of PVP-Pd nanoparticles was obtained.

Preparation of Pd/CMC-Fe^0 nanoparticles by Nano-palladium Deposition

Pd colloidal nanoparticles were added in the colloidal iron nanoparticles suspension prepared from 3.3.2 section. The mixture was stirred at room temperature for 1 h. The obtained iron Pd/Fe nanoparticles were separated from the mixture by centrifugation, washed several times with deionized water and ethanol before use or stored in dry methanol. Various ratios of Pd loading were prepared at 0.1, 0.2, 0.3, and 0.5 % loading.

2.5 Characterization of Zero-valent Iron Nanoparticles

The synthesized zero-valent iron nanoparticles and Pd modified zero-valent iron nanoparticles were characterized by various techniques. Electron microscope (TEM and SEM) was used to indentified particle size, shape and dispersion of the synthesized samples. The samples preparation for characterization was performed by dispersion into absolute ethanol using ultrasonication. TEM samples were prepared by placing a drop of colloidal dispersion of the synthesized Fe nanoparticles onto a carbon-coated copper grid followed by natural evaporation of the solvent. At least 100 nanoparticles were considered for reporting the mean diameter with standard deviation. The samples were prepared by pacing a drop of colloidal suspension of the synthesized Fe nanoparticles on stubs and let it dry at room temperature. EDX was connected to SEM for elemental analysis and elemental mapping. Structural characterization of the synthesized Fe nanoparticles was carried out by X-Ray powder diffraction. Surface composition of the particles was analyzed by Scienta X-ray photoelectron spectrometer. The prepared iron nanoparticle

samples were packed in aluminium foil bag under vacuum and then transferred into the sample cell. Hydrodynamic diameter of the synthesized Fe^0 nanoparticles was measured by dynamic light scattering method. The amount of Fe^0 samples dispersed in water was 2 g/L. The measured temperature is 25±0.1°C. The colloidal stability of the synthesized Fe^0 nanoparticles was analyzed from zeta potential.

2.6 Mobility and Stability of the Synthesized Zero-Valent Iron Nanoparticles

2.6.1 Dispersion Stability

The ability of colloidal iron nanoparticles suspended in the solution was preliminary monitored. 0.05 g of iron nanoparticles was dispersed in 10 ml of N_2 purged deionized water by ultrasonic bath. The colloidal suspension was kept in 10 mL vial in close system without headspace. Then, time that the particles start to segregate and settle at the bottom of vial was recorded.

2.6.2 Mobility

Mobility was determined by sand column experiment. The transport test of colloidal suspension was carried out with 10 cm high sand bed in a 10 mL syringe column. 0.05 g of the synthesized zero-valent iron nanoparticles was dispersed in colloidal form in 10 mL N_2 purged deionized water and filled on top of the soil bed. The eluent was collected at the bottom of the syringe column.

Section II Dechlorination of 1,2 Dichloroethane

Catalytic performance of the synthesized Fe^0 nanoparticles and Pd/Fe^0 bimetallic nanoparticles toward dechlorination of 1,2 dichloroethane contaminant in water was investigated in laboratory scale.

Batch experiments were conducted to test reactivity of the laboratory synthesized nanoscale particles for the dechlorination of 1,2 dichloroethane. The 5 ppm stock solution of 1,2-dichloroethane were prepared in the mixed solvent of less methanol and adding water for 1,2 dichloroethane at 5 ppm. The 20 ml headspace vial was filled with a suspension of desired amount of zero-valent iron nanoparticles (g of catalyst to a liter of

water; g/L). A cold solution of 5 ppm 1,2- dichloromethane was spiked in to into the catalyst suspension. Then, water was filled into the bottle with no headspace and sealed immediately with septum screw cap. The vial was placed on a rolling shaker for desired time. The speed of rolling and temperature were controlled at 70 rpm and 27±1°C, respectively). After rolling for desired time, the vial was cooled to 4°C. 10 ml of the solution was transferred by pipette to 20 ml headspace vial and immediately sealed with septum cap. Static headspace-solid phase micro extraction technique was applied to extract the remaining 1,2 dichloroethane. Polydimethylsiloxane (PDMS) was used as SPME fiber coating. The optimum extraction time was studied at 23±2ºC. The dechlorination reaction was studied at various conditions such as reaction time, the amount of catalyst (g/L) and concentration of 1,2 dichloroethane.

The concentration of 1,2 dichloroethane was determined by Hewlett Packard HP 5890 series II gas chromatograph. The GC was equipped with a flame ionization detector (FID) and a HP-5MS UI capillary column, 30m×0.32mm I.D.× 0.25 μm film thickness (Agilent). Ultrapure helium (99.999%) was used as the carrier with a flow rate 3 mL/min. Ultrapure nitrogen was used as make-up gas at initial flow rate 3 mL/min. H_2/air zero were used as fuel gas. The column oven temperature was maintained at 90°C. The detector temperature was fixed at 250°C. The injection port temperature was fixed at 200°C.

Section III A Case Study of Using Zero-Valent Iron Nanoparticles for Groundwater Remediation

Contaminant water samples were collected from 3 groundwater wells in Map ta Phut town, Muang District, Rayong Province. Sample 1 was collected from groundwater well in Map Ya community. Sample 2 and sample 3 were collected from groundwater wells in Neon Pha Yom community and Nong Nam Yen community, respectively. The collected samples were kept in plastic bottles and stored at 4°C. The chemical and physical quality of the groundwater such as pH, dissolved oxygen (DO) salinity were monitored and the amount of 1,2 dichloroethane was analyzed

CHAPTER 3

RESULTS AND DISCUSSION

Zero-valent iron nanoparticles and palladium-modified zero-valent iron nanoparticles were synthesized by different methods. Their particle size, morphology and composition were characterized by various techniques. The catalytic activity toward degradation of 1,2 dichloroethane was investigated. In addition, their dispersion stability, oxidation stability and the ability to transport in porous media was also explored. The results and discussion for all studied are shown in this chapter.

Section I Synthesis and Characterization of Zero-valent Iron Nanoparticles

In general, there are two strategies for nanoscale synthesis: top-down and bottom-up approaches. Top-down starts with large size of granular or microscale, the generation of nanoparticles via mechanical and/or chemical steps including milling, etching, and/or machining. Bottom up, the nanostructures were growth atom-by-atom or molecule-by-molecule via chemical synthesis, self-assembling and positional assembling. (Carroll et al. 2013). This work, zero-valent iron nanoparticles were synthesized by bottom-up approach via a chemical reduction method. Metal ion was used as a precursor and was reduced to metal atom by using a reducing agent. Normally, $NaBH_4$ was used due to strong reducing property. In addition, this method has been accepted as one of the most cost effective and a very simply method. It can be safely done in most chemistry laboratory with simple chemical reagents (He et al., 2005).

3.1 Synthesis of Bare Zero-valent Iron Nanoparticles

Zero-valent iron nanoparticles were synthesized in aqueous solution due to the environmental purposes**.** As zero valent nanoparticles are highly air-sensitive and easily oxidized to hydroxide or oxide forms, therefore the reduction reaction was carried out in nitrogen atmosphere. In addition, deionized water was purged with purified N_2 fall to the level below 3mg/L (~30 min). Hydrated $FeCl_3$ was use as Fe^{3+}precursor. Dissolving the precursor in water, the hydrated iron (III) solution was formed. After, BH_4^- is introduced

into Fe^{3+} solution, metallic iron was generated. The chemical reaction is shown in the following equation;

$$Fe(H_2O)_6^{3+} + 3BH_4^- + 3H_2O \longrightarrow Fe^0 + 3B(OH)_3 + 10.5H_2 \quad (3.1)$$

Due to the high charge density of Fe^{3+} in aqua complex, the O-H bonds became weakened and hydrolysis occurred (eq.3.2). The obtained solution is acidic. From the experiment, the pH of 0.01 M of $FeCl_3$ in aqueous solution was 2.69.

$$[Fe(H_2O)_6]^{3+}(aq) + H_2O(l) \longrightarrow [Fe(H_2O)_5(OH)]^{2+}(aq) + H_3O^+(aq) \quad (3.2)$$

In acid solution, it is possible that some of $NaBH_4$ introduced in the aqua iron complex will be consumed by H^+ reduction (eq.3.3) because of the higher electrode potential of $2H^+/H_2$ (eq.3.4) over that of Fe^{3+}/Fe^0 (eq. 3.5).

$$BH_4^- + H^+ + 3H_2O \rightarrow H_3BO_3 + 4H_2\uparrow \quad (3.3)$$

$$2H^+ + 2e^- \longrightarrow H_2 \qquad E^0 = 0.00\ V \quad (3.4)$$

$$Fe^{3+} + 3e^- \longrightarrow Fe \qquad E^0 = -0.04\ V \quad (3.5)$$

After an aqueous solution of $NaBH_4$ was added, gas bubbles immediately appeared, and the solution mixture turned from light yellow to black. The non-stabilized Fe particles agglomerated and precipitated nearly completely in a few minutes. The generated iron particles were harvested by centrifugation and washed with a large volume of nitrogen purged deionized water and ethanol. The obtained Fe particles were stored in dry methanol. SEM images of the particles are shown in Figure 3.1

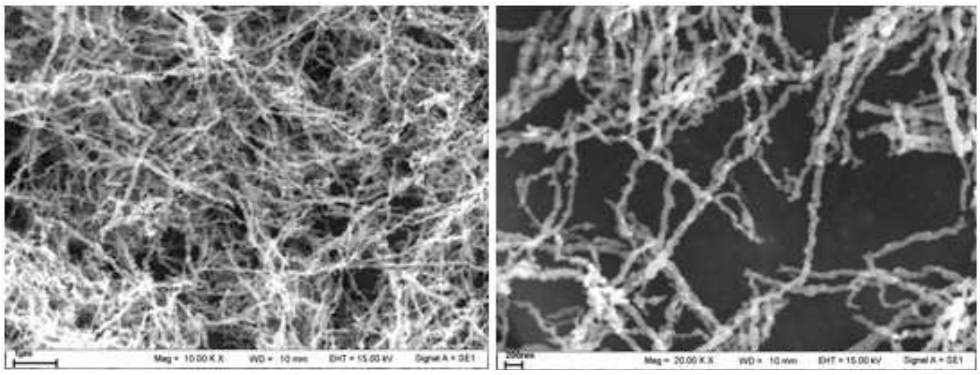

Figure 3.1 SEM images of bare iron nanoparticles prepared in the absence of stabilizers, using $NaBH_4$ as reducing agent.

According to the images, it can be seen that in the absence of the stabilizer, the resultant particles do not appear as discrete nanoscale particles but most particles formed chain-like aggregate. The diameter of the wires was around 60-140 nm and the length was more than 2.5 micron. In general, aggregation of magnetic metal nanoparticles takes place primarily through direct inter-particle interactions such as van der Waals forces and magnetic interactions (Sakulchaicharoen et al., 2010). Therefore, it is possible that after $NaBH_4$ was slowly added and Fe nuclei are continuously formed, the large magnetic interaction among Fe nuclei and /or the nanospheres would overwhelm the growth process of nanosphere, resulting in the formation of nanowire. Thus controlling rate of adding BH_4^- can prevent or decrease agglomeration of nanoparticles. It is well-known that zero-valent iron particle have a core–shell architecture which consists of metallic iron (Fe^0) form at the core while oxides and hydroxides form the shell as a result of oxidation of the iron surface (Carroll et al. 2013). Lu and co-workers showed that Fe-Fe_2O_3 core-shell nanowire and nanonecklace were obtained simply through controlling the reduction rate of Fe^{3+} ions by sodium borohydride. Nanowire was obtained when 2.0 M (1.52 g in 20 ML) of $NaBH_4$ was added in the aqua iron complex with rate 0.5 mL/s while nanonecklace was obtained when the adding rate was decreased to 0.02 mL/s. Our results, adding 2.0 M of $NaBH_4$ solution with flow rate 2 mL/s into 0.01 M of aqueous of Fe^{3+}, nanowire structure was obtained. It can be seen that, although slowly added BH_4^- and the concentration of Fe^{3+} precursor used extremely low, agglomeration and surface oxidation of the particle cannot avoid. Further improve surface area and surface stability is necessary (Lu et al., 2006).

3.2 Synthesis of Polymer-Stabilized Zero-valent Iron Nanoparticles

Nanoscale zero valent iron particles are colloid in nature and exhibit a strong tendency to aggregate. It can adhere to the surfaces of natural materials such as soil and sediment. To overcome this limitation and to improve their transport in porous media, researchers have used electrostatic and steric stabilization by adding stabilizers. An effective stabilizer should be able to specifically interact with the nanoparticles and hence suppress their growth. In addition for environmental applications, it should be benign, cost-effective and mobile in soils (B.Y. Yoo et al., 2007). In this work, CMC and water-soluble starch were selected as green-polymer stabilizers for the preparation of zero-valent iron nanoparticles.

3.2.1 Synthesis of CMC-Stabilized Zero-valent Iron Nanoparticles (CMC-Fe^0 Nanoparticles)

CMC-stabilized zero-valent iron nanoparticles were prepared under nitrogen atmosphere. Deionized water was purged with purified N_2 before using. After mixing of an aqueous solution of $FeCl_3$ and sodium methylcellulose (Na-CMC), an orange-brown color of carboxymethyl cellulose complex (CMC-Fe^{3+} complex) was obtained. Adding an aqueous solution of $NaBH_4$ into the mixture resulting in slowly changed the color to black of metallic Fe^0. This experiment, 40 times by mole of borohydride to Fe^{3+} was applied to accelerate the synthesis reaction. The obtained CMC stabilized Fe nanoparticles (CMC-Fe^0 nanoparticles) are colloidal dispersion without sedimentation to the bottom of reactor for longer than a week. The obtained CMC-Fe^0 nanoparticles were separated by centrifugation. The excess CMC was washed out by N_2 purged deionized water. In order to avoid further oxidation, the obtained samples were stored in colloidal form under dry methanol. The precipitated particles were easily re-dispersed in water by sonication.

CMC is a cellulose derivative with carboxymethyl groups (-CH_2-COOH) bound to some of the hydroxyl groups of the glucopyranose monomers of the cellulose backbone (Bajpai., 2015) (Fig. 3.2). It is an anionic linear polyelectrolyte, soluble in cold water. CMC is low-cost and environmentally friendly. There are number of literatures reported on using of CMC as stabilizer for the preparation of iron nanoparticles (Lin et al., 2010). The reports indicated that both carboxylate group (-COO-) and hydroxyl group (-OH) of CMC can interact strongly complexes with Fe^{3+} ions in solution, thereby preventing agglomeration of Fe^0 nanoparticles (Cirtiu et al., 2011).

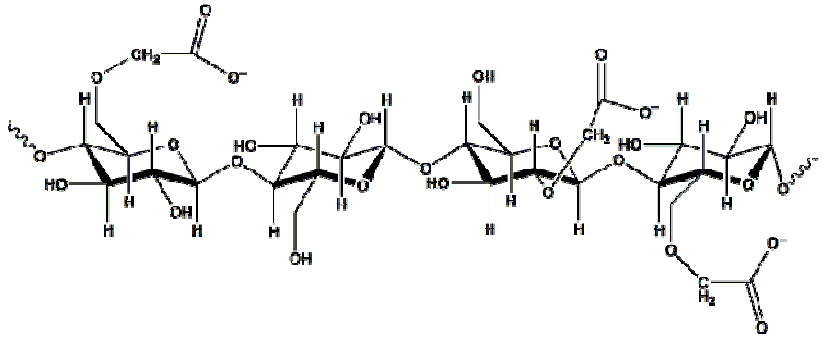

Figure 3.2 CMC structure based on the β-(1⟶4)-D-glucopyranose polymer of cellulose (Chaplin, 2014).

Although, the structure of CMC consists of carboxylate group which can strongly interact with Fe^{3+} precursor. However, the level of interaction depends on media system such as pH and basic strength. From the experiment, the pH of CMC-Fe^{3+} complex with contains 0.01M of Fe^{3+} was about 4.5. The mixture was a yellow solution. However, 5% of NH_4OH solution was slowly added into the mixture to control pH of the reaction, the color changed to orange and slightly turned to orange-brown at high pH. The interaction between CMC and Fe^{3+} would indicate the stability of further obtained nanoparticles. UV-visible spectroscopy of CMC-Fe^{3+} complex was used to study interaction of the complexes. The results are shown in Fig. 3.3

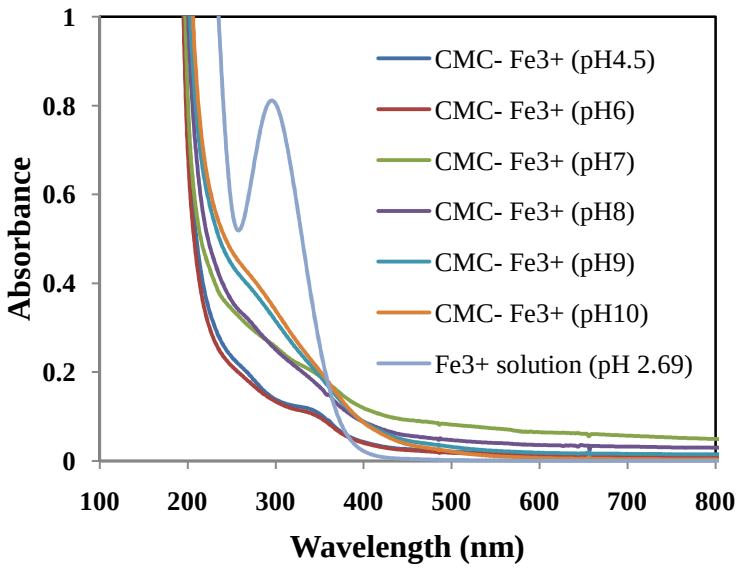

Figure 3.3 Absorption spectra of CMC-Fe^{3+} complexs at different pH.

From Figure 4.3, a broad peak with maximum wavelength at 298 nm is assigned to hexa-coordinated aquo complexes of various forms such as of $Fe(H_2O)_6^{3+}$, $Fe(H_2O)_5(OH)^{2+}$, $Fe(OH)_4(OH)_2^{+}$ and $Fe(H_2O)_3(OH)_3^{0}$. The pH of the solution was 2.69. When CMC was mixed, CMC-Fe^{3+} hydrate complexes were form. pH of the mixture changed to about 4.5. The absorption spectrum of the mixture displayed a nearly exponential decaying profile as the wavelength increases. This observation indicates the intermolecular hydrogen bond between Fe^{3+} aqua complex and COOH / OH species on CMC-Fe^{3+} complex. An increase pH of CMC-Fe^{3+} complex by adding NH_4OH, the intensity of the absorption spectrum increased. Thus CMC-Fe^{3+} complex concentration is function of pH.

As the pKa value of CMC has been reported to be ~ 4.3 (He, 2007). Thus, at pH lower than 4.3 the most of CMC ligand remain protonated (OH dominant) and only few binding sites might be available for Fe^{3+} ions. Whereas, increasing the pH above 4.3, the deprotonation (–O– dominant) increases, providing more binding sites for Fe^{3+}. Cross-link network would be formed. It was suggested the more stable complexes will be obtained in basic solution due to stronger interaction between Fe^{3+} and COO^- than acid solution, resulting in high stability of CMC-Fe^{3+} complex. From Fig. 3.3, at pH 5-7, a shoulder at 298 nm of the remaining Fe-aqua complex was stilled observed but the intensity was decreased. At pH 8, this shoulder peak disappeared. It is implied that, all or almost free aqua complex of Fe^{3+} would be formed complex with CMC at this pH. Therefore, the carboxylic groups of CMC are expected to be almost fully disassociated and strongly bind with Fe–O–. According to Hosny et al. (1997), CMC-Fe^{3+} complex can be described by a single general chemical formula $[(CMC)FeCl.H_2O]Cl.2H_2O$. At higher pH (9 and 10), the color of solution started to change from orange to reddish brown. It is possible that at high concentration of OH^-, the formation of hydroxides species such as CMC –Fe-(OH) occurred. These species would diminish the reduction of Fe^{3+} and nucleation of Fe atom. A suitable pH which CMC strongly interact with the Fe^{3+} ions and low hydroxide complex formation should be controlled. Thus, suitable pH which CMC strongly interact with the Fe^{3+} ions in the solution and low hydroxide species formation should be around 7-8.

The particle size and morphology of the obtained CMC-Fe nanoparticles were characterized by electron microscopy technique. The TEM images obtained from the samples prepared at 5 (Fig. 3.4) and pH 8 (Fig. 3.5) are shown. Reaction conditions were carried out at room temperature for 6 hour, the concentration of Fe^{3+} precursor is 0.01M.

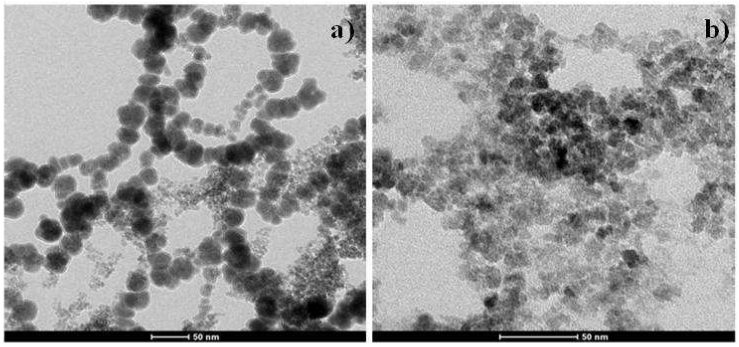

Figure 3.4 TEM images of CMC-Fe^0 nanoparticles prepared at pH 5 a) at lower magnification b) at higher magnification expand from small particle areas. The reaction

was carried out at room temperature for 6 h. Concentration of Fe^{3+} precursor was 0.01M. Mole ratio of Fe^{3+}: CMC (monomer) was 1:10. Mole ratio of BH_4^- to Fe^{3+} was 1: 40

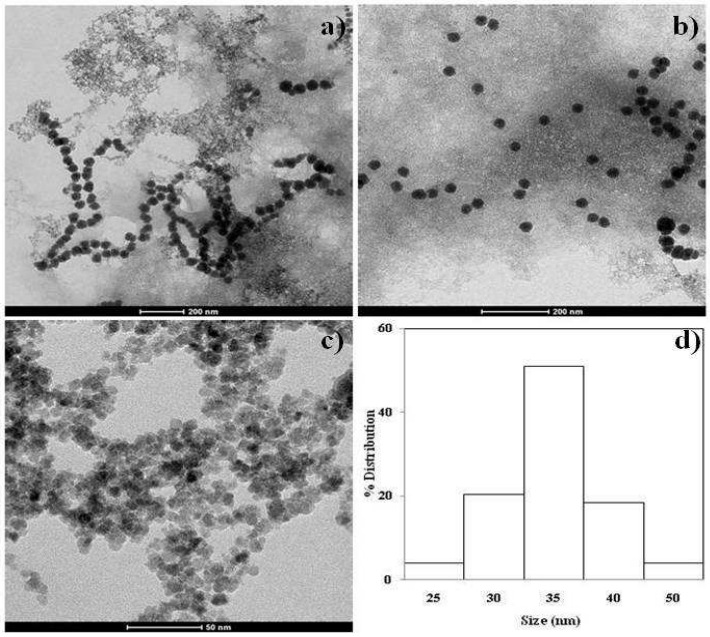

Figure 3.5 TEM images of CMC-Fe^0 nanoparticles prepared at pH 8 a) at lower magnification b) higher magnification c) higher magnification expand from small particle areas and d) particle size distribution histogram. The reaction was carried out at room temperature. Concentration of Fe^{3+} precursor was 0.01M Fe^{3+}. Reaction time was 6 h. Mole ratio of BH_4^- to Fe^{3+} was 1: 40. Mole ratio of Fe^{3+} to CMC (monomer) was 1:10.

From the images in Figure 4.5, there are 2 groups of particle sizes were obtained. The larger particles are 33.74±4.96 nm in diameter while the smaller sizes of particles are 8.20±1.38 nm. It is possible that during the preparation method CMC solution and Fe^{3+} solution were not homogeneous mixing due to high viscosity of CMC. It can be confirmed that CMC played an important role in stabilizing iron nanoparticles. Clearly discrete and well-dispersed particles were obtained, although some agglomeration to chain like particle was still observed. In comparison, the sample prepared in acid media at pH around 5 has wide range of particle size distribution than the samples prepared at pH = 8. It is possible that a large particle of Fe formed at low pH dues to weak CMC-Fe^{3+} interaction.

To elucidate the stabilization mechanisms of CMC-Fe^0 nanoparticles, further insight into the interactions between the CMC and Fe^0 nanoparticles, infrared spectroscopy was studied. The FT-IR spectra of CMC and CMC-Fe^0 nanoparticles are shown in Fig. 3.6

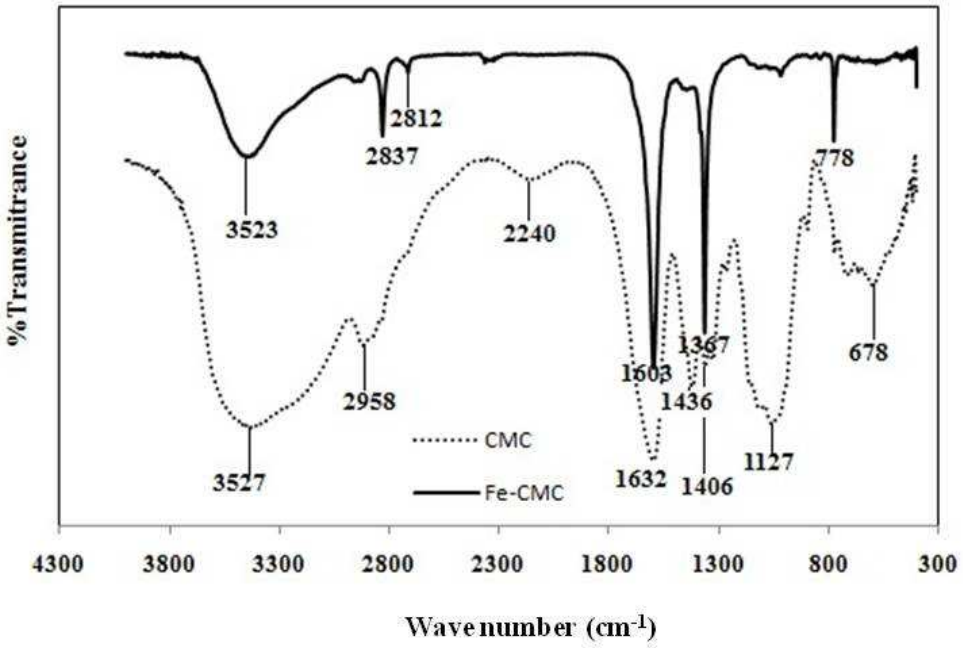

Figure 3.6 FT-IR spectra of CMC and CMC-Fe^0 nanoparticles.

From the spectrum of bare CMC, the wide band observed at 3527 cm^{-1} can be attributed to O-H stretching of glucopyranose and its width was ascribed to the formation of inter and intramolecular hydrogen bonds (Lin et al., 2010). The bands at 2958 cm^{-1} were attributed to the asymmetric stretching of C-H. The band at 1632 cm^{-1} and 1436 cm^{-1} was ascribed to $–COO^-$ asymmetric stretching and symmetric stretching, respectively. The C-O ether bond shows stretching at 1265 cm^{-1} while the C-O alcohol bond shows stretching at 1127 cm^{-1}. In comparison between the spectrum of CMC and CMC-Fe nanoparticles, the absorption bands of CMC-Fe nanoparticles are sharper. The stretching frequencies of symmetric and a symmetric –COO- are shift to lower wavelength. The $–COO^-$ asymmetric stretching and symmetric stretching was found at the band at 1632 cm^{-1} and 1436 cm^{-1}, respectively. In addition, it is interesting that the band at 1127 cm^{-1} becomes very weak. These changes indicate strong interaction between Fe and hydroxyl and carboxylate group of CMC which imply to the stability of CMC-Fe^0 nanoparticles.

The structure of CMC contains abundance of –OH groups. This type of hydrogen bonding could be important in binding CMC onto Fe nanoparticles although the individual bond strength may not be as strong as that between Fe and the carboxylate groups. For carboxylate groups, three modes of adsorption configurations such monodentate chelating, bidentate chelating and bidentate bridging can be formed with Fe as shown in Fig. 3.7.

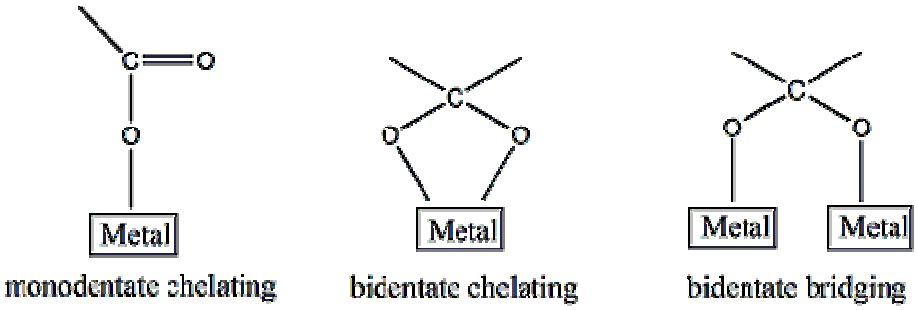

Figure 3.7 Mode of adsorption of carboxylate groups (Lin et al., 2010).

It is difficult to identified mode of adsorption which depends on their particle size and surface structure. The separation of the symmetric and asymmetric carboxylate positions (Δν) for pure stabilizer and stabilized zero-valent nanoparticles could help to identify the adsorption configurations. If Δν = 200-320 cm^{-1}, the binding is governed by monodentate interaction. If Δν <110 cm^{-1}, it is bidentate chelating interaction, and if Δν =140-190 cm^{-1}, it is by bidentate bridging. As shown in Figure 4.6, it is evident for CMC that there is no carbonyl stretch (C=O, at 1720 cm^{-1}) along the spectrum. However, there is a slight asymmetric COO-strength shift from 1624 to 1603 cm^{-1} and a symmetric COO-strength shift from 1436 to 1367 $cm^{-1.}$ The Δν stabilized Fe^0 is 236 cm^{-1} (1603–1367 = 236 cm^{-1}). From the results, it is possible that the binding mode between CMC and Fe^0 should be monodentate chelating as shown in Figure 3.8.

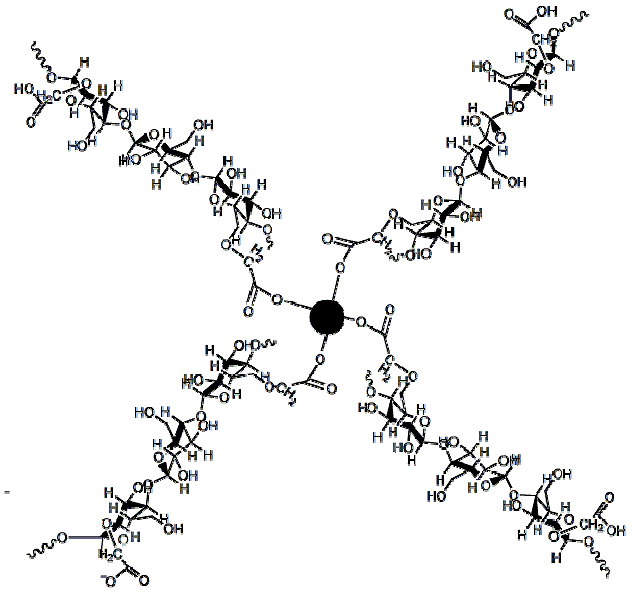

Figure 3.8 Proposed of interaction between CMC and Fe atom on CMC-Fe^0 nanoparticles.

Our results are consistent with the report of He and co-worker (He et al., 2007) which reported that monodentate chelating is the primary mechanism for binding CMC molecules to Fe nanoparticles. However, the result is not consistent with the results reported from Lin and co-workers (Lin et al., 2010) which proposed bidentate bridging. The reason for this differs may be possibly due to the influence of pH and ionic strength of the solution

3.2.3 Synthesis of Starch-stabilized Zero-valent Iron Nanoparticles (STR-Fe^0) Nanoparticles)

Zero-valent iron nanoparticles were also synthesized by using soluble starch as a stabilizer. Soluble starch is a low-molecular-weight carbohydrates produced by the hydrolysis of starch. The structure is made up of two types of polymers: amylose and amylopectin. Amylose is a linear homopolymer of α-1,4 –linkaged glucose. Amylopectin is highly branched form amylose. The linear α-1,4 –linkaged glucose backbone is branched by an α-1,6 –linkaged (Jane et al., 1999). The structure of amylase and amylopectin are shown in Fig. 3.9.

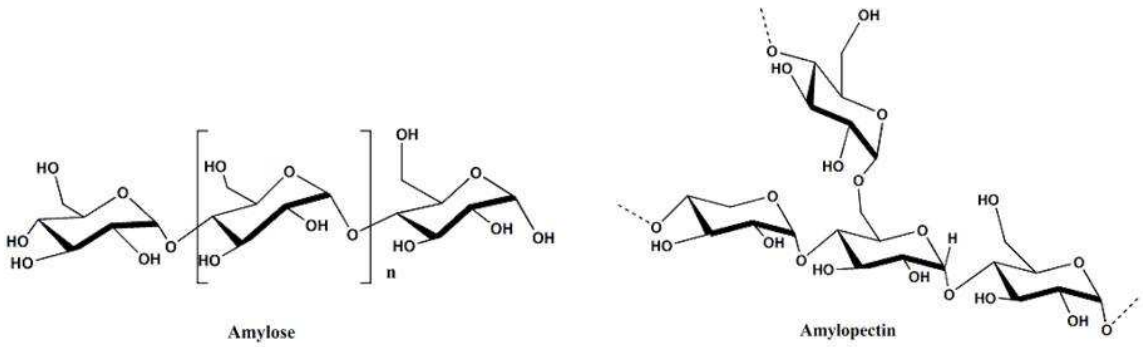

Figure 3.9 structures of amylose and amylopectin.

It is expected that when exposed starch into to the solution of ferric ions, the hydroxyl groups extensively present in starch will facilitate the complex of ferric ions to the molecular matrix. Starch hydroxyl group would be expected to become increasing ionized with an increasing pH. As pKa of starch is ~12, thus at pH lower 12, most of hydroxyl groups will be in protonate form. The optimum pH for the preparation of Fe nanoparticles with different pH was studied by UV-visible spectroscopy. The results are shown in Fig. 3.10.

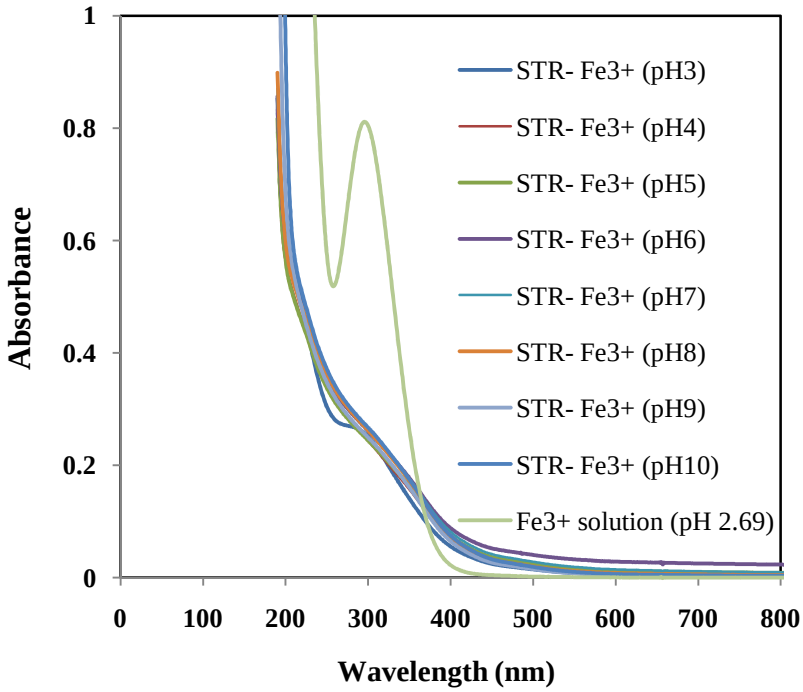

Figure 3.10 UV-visible spectra of starch-Fe^{3+} complexes at various pH.

According to Fig. 3.10, a broad peak at maximum wavelength 298 nm is assigned to hexa-coordinated aqua complexes. The pH measuring from the mixture of Fe^{3+} solution and starch solution is 2.9. The absorption band of the sample at this pH showed monotonic decaying profile of hydrogen bonding between an aqua complex of Fe^{3+} and OH group on starch. As a shoulder peak at 289 nm wavelengths suggested the free Fe^{3+} hydro complex. At higher pH than 3 this shoulder disappeared.

TEM images of starch-Fe iron nanoparticles prepared at room temperature and at 60°C are shown in Figure 3.11- 3.12.

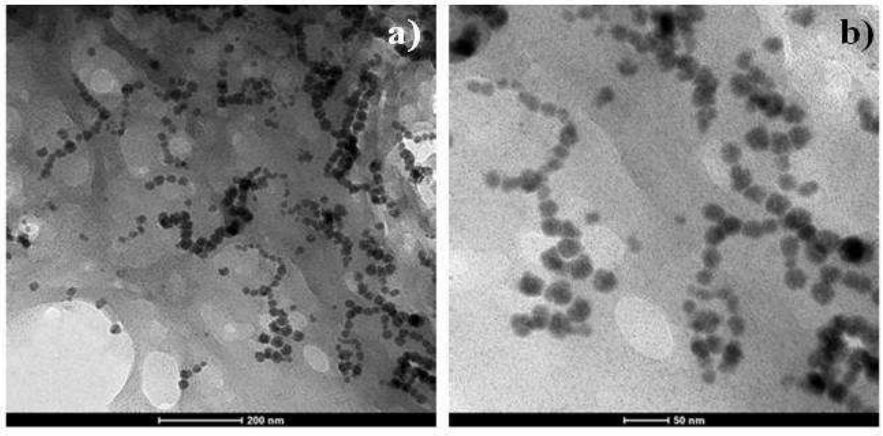

Figure 3.11 TEM images of STR-Fe^0 nanoparticles prepared at room temperature. Concentration of Fe^{3+} precursor was 0.01M. Reaction time was 6 h. Mole ratio of BH_4^- to Fe^{3+} was 1: 120. Ratio of Fe^{3+} to starch (monomer) was 1:10.

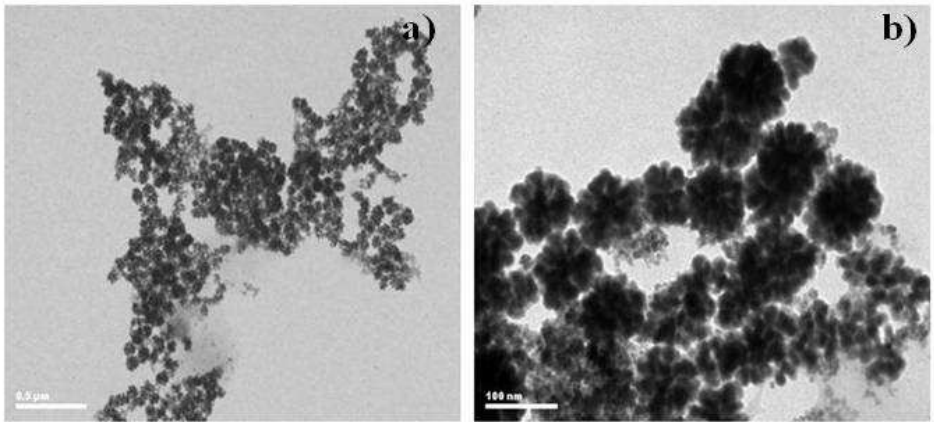

Figure 3.12 TEM images of STR-Fe^0 nanoparticles prepared at 60 ^oC. Concentration of Fe^{3+} precursor was 0.01M. Reaction time was 6 h. Mole ratio of BH_4^- to Fe^{3+} was 1: 40. Ratio of Fe^{3+} to starch was 1:10.

Figure 3.11 demonstrated that the obtained STR-Fe^0 nanoparticles are discrete particles without chain like aggregation. The average particle size was 83.75±20.56 nm. From the study of starch-Fe^{3+} complex, deprotonation of OH group and coordination between Fe and –CO- in starch would not occur at pH 8. Thus, the stability of starch-Fe nanoparticles may from the formation of intramolecular hydrogen bonding of its structure. Hydroxyl groups of starch may act as the passivating contacts, thereby preventing the resultant nanoparticles from agglomeration (He & Zhao, 2005).

Figure 3.12 showed many finer nanoparticles with sizes of 17±5 nm were packing together into larger particles with sizes of 70-90 nm. It is possible that the primary iron (17

nm) assembled itself into spherical secondary irons (70-90 nm) due to the excess of stabilizer and Ostwald ripening (Zhong et al., 2006). The formation of intra-starch iron clusters played a fundamental role in nanoparticle dispersion and stabilization. Thus the preparation at high temperature (at 60°C), smaller particles will be obtained but more tendency to aggregate.

From the experiment, it was noticed that using starch as stabilizer, higher ratio of $NaBH_4$ to Fe3+ was required in order to complete reduction. It is possible that at pH 8, OH-Fe^{3+}- intramolecular hydrogen bonding was formed. This would diminish rate of the reduction reaction. Thus, the reduction of HO-Fe^{3+} to Fe^0 required plenty amount of BH_4^- and take longer time compare to reduction of Fe^{3+}-CMC complex. In order to elucidate the stabilization mechanisms of STR-Fe^0 nanoparticles, infrared spectroscopy was studied. The FT-IR spectra of starch and STR-Fe^0 nanoparticles are shown in Fig. 3.13.

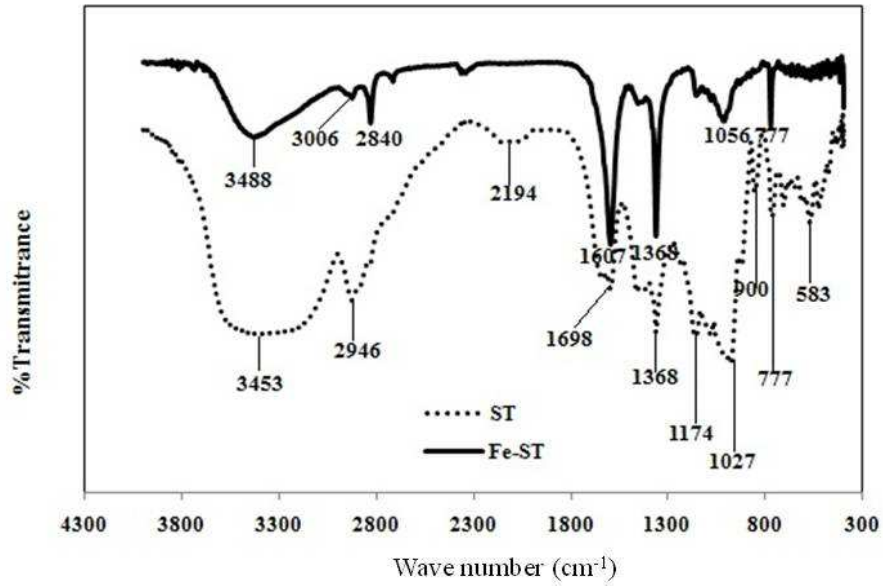

Figure 3.13 FT-IR spectra of pure starch and STR-Fe^0 nanoparticles.

According to the spectrum of pure starch, the wide band observed at 3348 cm^{-1} can be attributed to the O-H stretching of glucose and its width was ascribed to the formation of inter and intramolecular hydrogen bonds. The bands at 2935 and 2887 cm^{-1} were attributed to the asymmetric stretching of C-H, while the band at 1656 cm^{-1} was ascribed to adsorbed water and the bands at 1421 and at 1357 cm^{-1} to the angular deformation of C-H. The C-O ether bond shows stretching at 1174 cm^{-1} while the C-O alcohol bond shows

stretching at 1027 cm^{-1}. Compared with the spectrum of STR-Fe^0 nanoparticles, the strongest band at 1174 and 1027 cm^{-1} becomes a very weak signal. These indicated the interaction between Fe^{3+} and hydroxyl group. There has been reported studied on the interaction between alkoxy groups on starch and Fe^{3+} through electron paramagnetic resonance (EPR) and conductivity measurements (Ciesielski et al., 2003). The results suggest that the iron-starch interactions and formation of intra-starch. Fe clusters play a fundamental role in dispersing and stabilizing the iron nanoparticles. OH group on starch was not only adsorbed to the Fe^0 surface but also formed a gel network through hydrogen bonding so that the gel network structure can also trap colloidal particles to stabilize dispersions. The interaction between starch and Fe atom on STR-Fe^0 nanoparticles are shown in Fig. 3.14.

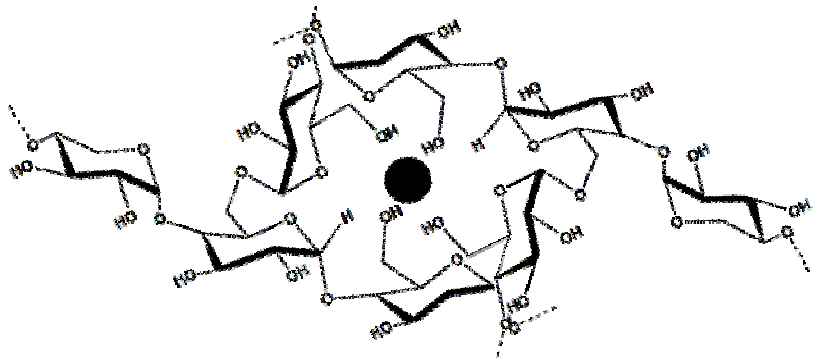

Figure 3.14 Proposed of interaction between STR and Fe atom on STR-Fe^0 nanoparticles.

3.2.4 The Effect of Reaction Parameters

As, the properties of nanoparticles depend on their particle size. Thus controlled synthesis of the particle size and distribution are important. Particle size and morphology of nanoparticles can be controlled by changing reaction parameters such as reaction temperature, time, heating rate, concentration of the metal precursor and the stabilizer ratio. This work, the effect of reaction temperature, reaction time, concentration of Fe^{3+} precursor and ratio of Fe to CMC stabilizer was studied. Reaction temperature was studied at room temperature and 60°C. Mole ratio of Fe precursor to CMC (monomer) was studied at 1:5 and 1:10 (CMC). Concentration of Fe^{3+} precursor was studied at 0.01 M and 0.02 M. Reaction time was studied between 2-10 h. TEM images of the samples obtained at different reaction parameters are shown in Figure 3.15-3.19.

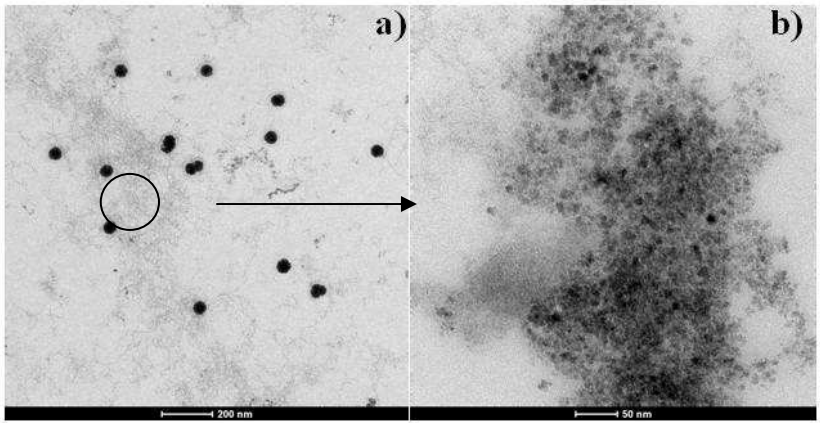

Figure 3.15 a) TEM images of CMC-Fe^0 nanoparticles synthesized at room temperature for 4 h, 0.01 M Fe^{3+}, 1:5 mole ratio of CMC (monomer)/Fe^{3+} b) high magnification image of Fig. a) focusing on the small particle areas.

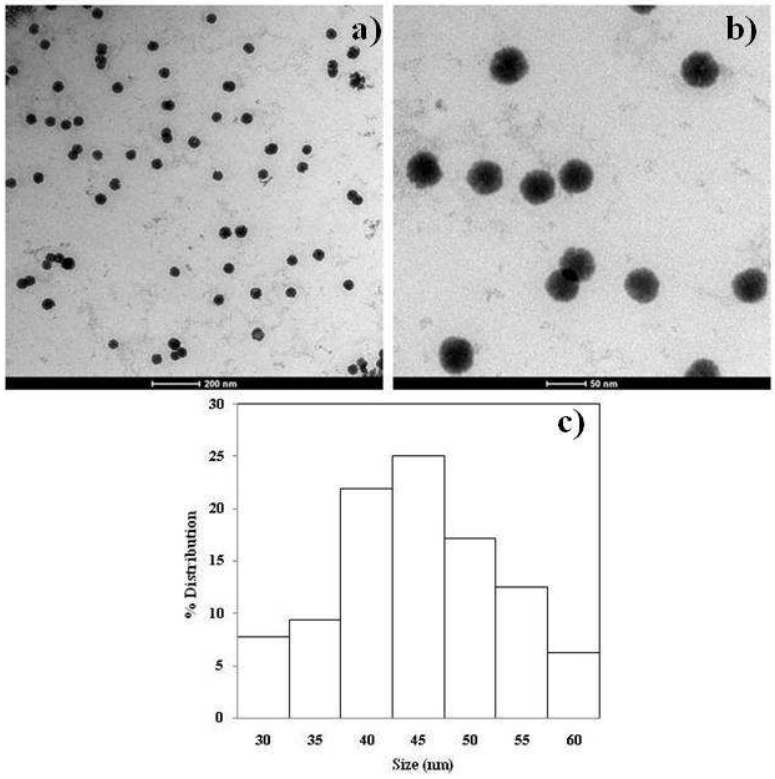

Figure 3.16 a) TEM images at low magnification and b) at high magnification of CMC-Fe^0 nanoparticles synthesized at room temperaturefor 6 h, 0.01 M Fe^{3+}, 1:5 mole ratio of CMC (monomer) to Fe^{3+} c) histogram of particle size distribution.

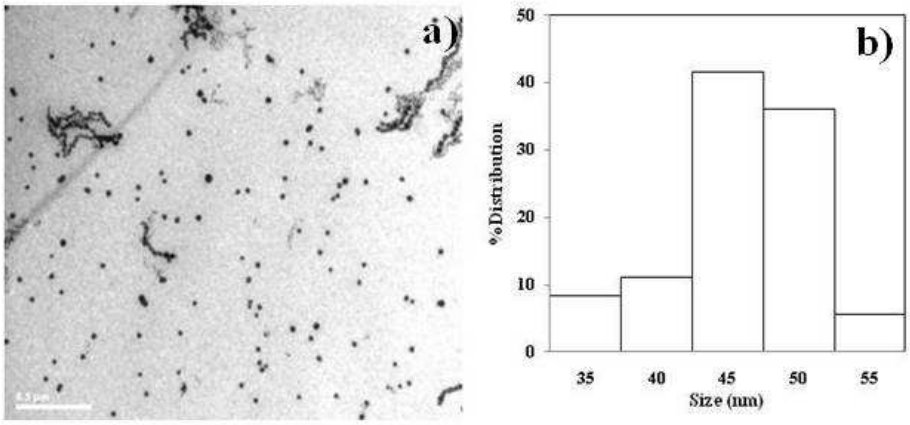

Figure 3.17 a) TEM images of CMC-Fe^0 nanoparticles synthesized at room temperature for 10 h, 0.01 M Fe^{3+}, 1:5 mole ratio of CMC (monomer)/Fe b) histogram of particle size distribution.

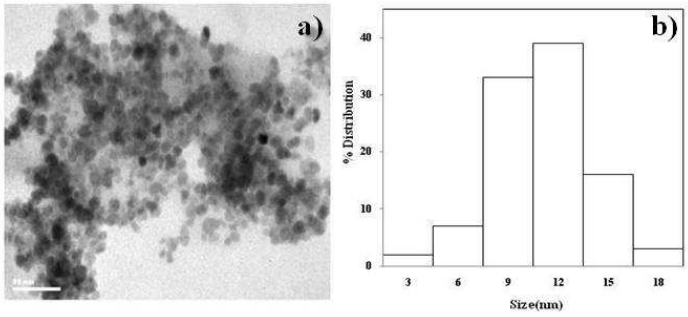

Figure 3.18 a) TEM images and histograms of particle size distribution of CMC-Fe^0 nanoparticles synthesized at 60 ˚C for 2 h, 0.01 M Fe^{3+} 1:10 mole ratio of CMC (monomer)/Fe b) histogram of particle size distribution.

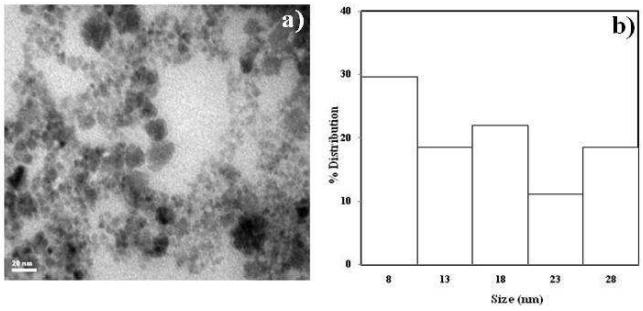

Figure 3.19 a) TEM images of CMC-Fe^0 nanoparticles synthesized of 0.02 M Fe^{3+} precursor. The reaction was carried out at 60 ˚C for 2 h, mole ratio of CMC (monomer)/Fe^{3+} was 1:10 b) histrogram of particle size distribution.

Reaction time was clearly affected to the particle size of Fe^0 nanoparticles as shown in Figure 4.15-4.17. At the reaction time of 4 h. the obtained particles seem to be an

amorphous structure with poor crystalline. While leaving to 6 h, larger size of particles with clear boundary of crystalline structure was obtained. However, some amorphous particles with no clear boundary were still obtained. Increasing the reaction time to 10 h, the small particle of amorphous seems to grow to crystalline spherical particles. In addition, it can be noticed that longer reaction time the particles tend to aggregate to chain like particles.

It has been known that stabilizer not only plays an important role in protect nanoparticles from aggregation but also in sized control synthesis (He & Zhao, 2007). For CMC-Fe nanoparticles prepared from molar ratio 1:5 and 1:10 (Fig. 4.15 and 4.16), I was found that an increase in the ratio to 1:10, the average particle size was significantly decrease and less aggregration. In addition, it is clearly showed that increase reaction temperature from room temperature to 60°C (Fig 4.15 and 4.18), smaller in size of the particle was obtained. Only 2 h of reaction time, clearly spherical particles was obtained. This effect is due to an acceleration of the growth rate with an increase in reaction temperature.

The images in Fig. 3.18 and 3.19 clearly showed that the particle sizes and morphology depend on the ion precursor concentration. The average particle size was increase when the concentration of Fe^{3+} precursor was increased. As the results, it can be concluded that the optimum Fe^{3+} precursor for the preparation of zero-valent iron nanoparticles is the 0.01M.

3.3 Synthesis of Zero-valent Iron Nanoparticles on Material Support

Immobilizing of zero-valent iron nanoparticles in or on supports provides an alternative solution to overcome the stability. This research, zero-valent iron nanoparticles were synthesized in the presence of mesoporous silica nanoparticles and activated carbon as support materials.

3.3.1 Synthesis of Mesoporous Silica Nanoparticles

Mesoporous silica nanoparticles were synthesized following the report of Shi, et al., 2010 (Shi et al., 2010). The reaction was carried out in an extremely dilute solution and extremely low concentrations of TEOS (4.42 M) and CTAB (0.0057M). The

morphology and particle size of the synthesized silica nanoparticles were analyzed by transmission electron microscopy as shown in Fig. 3.20.

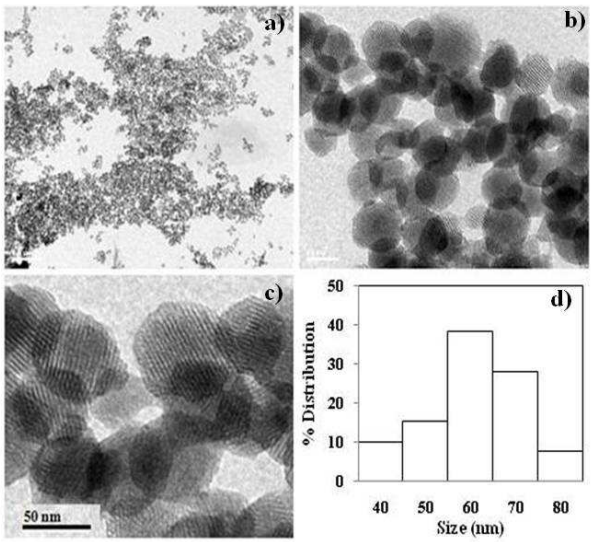

Figure 3.20 a-c) TEM images at different magnifications and histogram of particle size distribution of mesoporous silica d) histogram of particle size distribution

According to the images in Fig. 3.20 monodisperse spherical particles with porous structures were obtained. The average particle size diameter was 58 ±10 nm. The pore diameter estimated from the images is about 3.3 nm. Regular arrangement of cylindrical mesoporous that form a one-dimensional pore of hexagonal arrays was obtained. These results indicated the typical MCM-41 structure. Both top and side views obtained from TEM images indicated the three dimensional images of crystallized mesoporous silica. The highly ordered mesoporous silica consists of the gathering of rod-like silicates. The cross sectional patterns showed hexagonal structure which is the distinctive feature of mesoporous silica.

Schematic diagram synthesis of mesoporous silica is shown in Fig. 3.21. cetyltrimethylammonium bromide (CTAB) as surfactant template was used to form liquid crystalline micelles in an aqueous solution under basic conditions. TEOS was added to this micellar solution to make, upon hydrolyses and condensation, a silica network around the micelles. Under these conditions the ionic surfactants form spherical micelles which form supramolecular aggregates of micellular rods that act as templates. The hydrolysis and condensation of silica precursors, TEOS forms a solid silicate mesostructure around the template due to electrostatic interactions between the negatively charged silica species

and positively charged of the surfactant. Removal of the organic template by thermal treatment yields a mesoporous silica, hexagonally ordered silica framework was formed.

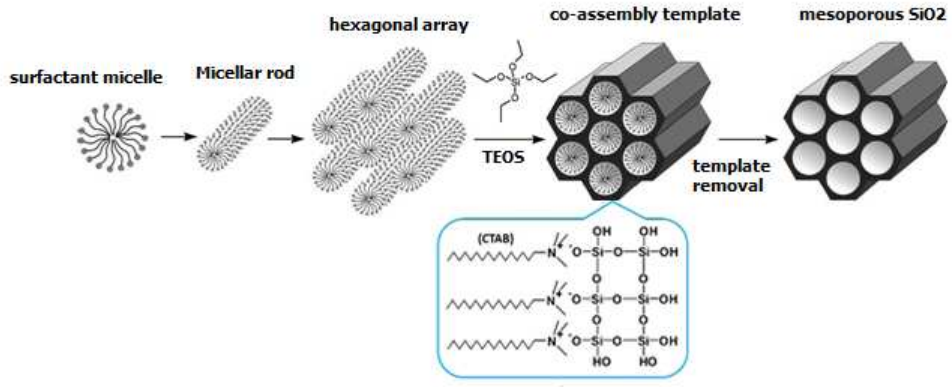

Figure 3.21 Proposed mechanism of mesoporous silica formation (Alahmadi, 2012).

3.3.2 Zero-valent Iron Nanoparticles on Mesoporous Silica Nanoparticles (Fe^0/SiO_2 Nanoprticles)

Nanoscale zero-valent iron supported on mesoporous silica was synthesized via a wet-impregnation route followed by the chemical reduction of Fe^{3+} with $NaBH_4$. Particle size and morphology of the obtained Fe^0/SiO_2 nanoparticles were characterized by TEM techniques. The obtained images are shown in Fig. 3.22.

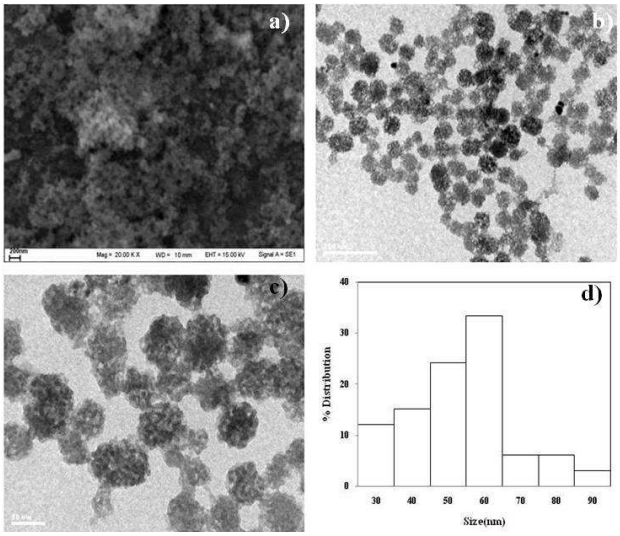

Figure 3.22 a) SEM image b-c) TEM image at different magnifications of the synthesized Fe^0/SiO_2 nanoparticles with 10% Fe loading.d) histogram of particle size distribution.

According to the images in Figure 3.22, collapse of the structure of mesoporous silica after adding Fe particles were observed. The mean diameter of the obtained Fe^0/SiO_2 particles was 60±10 nm. A few chains like of bare Fe particles were observed. This experiment, 10% of Fe loading on silica was obtained (EDX analysis). At this % loading, the destruction of MCM-41 can be noticed. This may results from the dissolution of MCM-41 framework due to low pH of Fe^{3+} solution or from the reaction between $NaBH_4$ and water. There are only few literatures reported on loading Fe on MCM-41. Petala and co-worker synthesized nanoscale zero-valent iron supported on mesoporous silica (Petala et al., 2013). The synthesis method was based on borohydride reduction and use of a $FeCl_3$ impregnating silica mesoporous matrix of MCM-41 material in ethanol medial. This TEM images showed, at 9.3% Fe loading, the elliptical in shape of Fe particles with a maximum size of about 80 nm randomly distributed and immobilized on the mesoporous silica surface. MCM-41 structure retains its ordered structural characteristics. Although, the preparation method is similar, however the obtained images are different. It is possible that the concentration of Fe added in our experiment is high resulting in leaching of silica.

4.3.3 Zero-valent Iron Nanoparticles on Activated Carbon (Fe^0/C Nanoparticles)

Activated carbon is a well known adsorbent due to its high surface area and porous structure. It can be used to adsorb gases and compounds dispersed or dissolved in liquids. As, the efficiency of the adsorption is strongly dependent on their surface chemical features, therefore, the surface chemical modification of carbon is required. This work, modified activated carbon was prepared by HNO_3 treatment. There surface structure was characterized by FT-IR spectroscopy. The FT-IR spectra are shown in Figure 3.23.

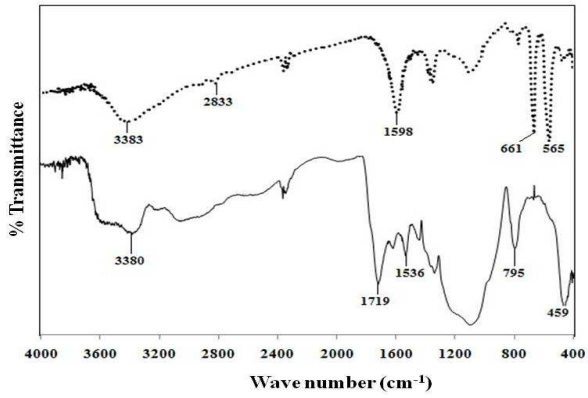

Figure 3.23 FT-IR spectra of a) activated carbon b) after pretreatment with HNO_3.

Infrared spectroscopic analyses of the HNO_3 treated carbons showed strong absorption at approximately 1719 cm^{-1} (-C=O), 1536 cm^{-1} ($-COO^-$), 1250 cm^{-1} (-C-O) and 3380 cm^{-1} (-OH) which can be assigned to carboxylic acid groups. In comparison between the activated carbon, much high intensity of COO^- was obtained.

Zero-valent iron nanoparticles on activated carbon support were prepared by chemical reduction-deposition method. It involves mixing of activated carbon and metal precursor with stirring to ensure maximum metal dispersion in the solution. The oxygen groups on the carbon surface are expected resulting in an increase loading and further improving the Fe dispersion. As a delicate optimization of carbon surface chemistry is needed to achieve optimal interaction between the carbon support and Fe precursor, this work, pH of the mixed solution Fe^{3+} and carbon was adjusted to 8. After slowly added an aqueous solution of $NaBH_4$, Fe^{3+} ions were reduced into Fe^0 clusters deposited on carbon support.

Morphology and particle size distribution of the obtained carbon supported Fe nanoparticles was analyzed by TEM and SEM techniques. The images are shown in Fig. 3.24.

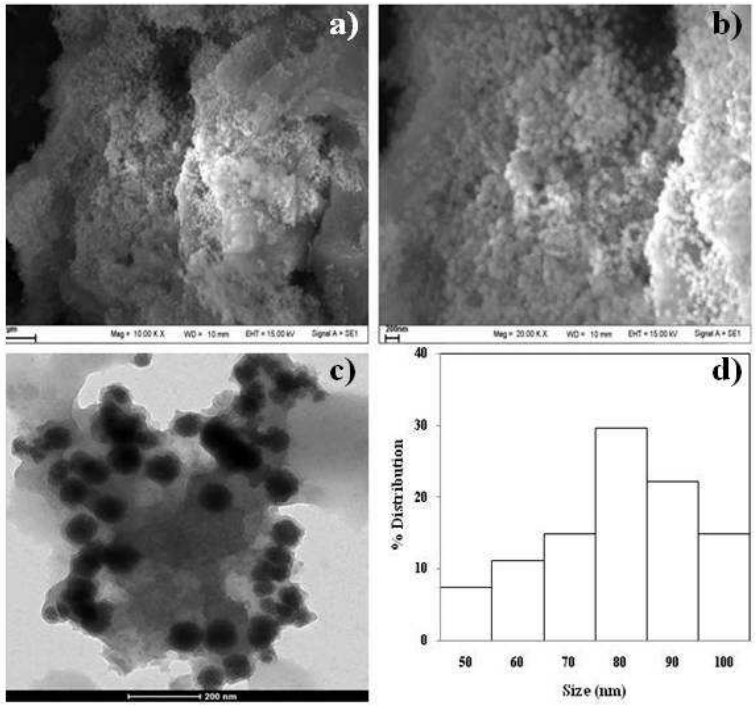

Figure 3.24 a), b) SEM images c) TEM image of the synthesized Fe^0/C nanoparticles d) histogram of particle size distribution of Fe^0/C nanoparticles.

From SEM images, a spherical in shape of the Fe nanoparticles on the carbon support surface was obtained. The particles are well dispersed with narrow size distribution. From TEM images, the average dimension was 75±13 nm. After treatment, the polar functional groups on carbon surface such as hydroxyl are more accessible to Fe^{3+} precursor during reduction from aqueous solutions. In basic solution (pH 8), deprotonation of hydroxyl group and carboxylate group enhanced an interaction of Fe^{3+} precursors or Fe nanoparticles with the carbon support and thus minimize the metal sintering. The particles size and morphology of the synthesized zero valent iron nanopartiles for all reaction parameters are shown in Table 4.1.

Table 4.1 Average particles size and morphology of the synthesized zero-valent iron nanoparticles.

Sample	Average particle size TEM (nm)	Morphology
Bare Fe^0	Width 60-140 nm length 2.5 micron	Chain-like aggregate.
CMC-Fe^0 (prepared at room temperature)	8.2 - 45 nm	Discrete particles
CMC-Fe^0 (prepared at 60°C)	12 nm	Discrete particles
STR-Fe^0	17 nm , 70-90 nm	Discrete particles with some clusters agglomeration
Fe^0/SiO_2	60 nm	embedded in Silica
Fe^0/C	75 nm	discrete particle with some aggregation

3.4 Synthesis of Pd-Modified CMC-stabilized Iron Nanoparticle (Pd/CMC-Fe^0 Nanoparticles)

In general, bimetallic nanoparticles can be prepared by successive reduction and simultaneous reduction. Successive reduction is consecutive reduction of the second metal ions and subsequent deposition onto the first metal particle while co-reduction is simultaneous reduction of two metal ions. This method results in the formation of core/shell structure nanoparticles, while the simultaneous reduction, the formation of alloy structure nanoparticles was obtained. In this experiment, Pd-modified Fe^0 bimetallic

nanoparticles were prepared by 2 two step reaction; namely palladization and nano-palladium deposition.

3.4.1 Palladization Method

CMC-Fe^0 nanoparticles were firstly prepared. Then, known quantities of $Pd(NO_3)_2$ was loaded into to the aqueous suspension of Fe^0 nanoparticles. Autocatalytic reduction of $Pd^{2+}$and oxidation of Fe^{3+} was happened due to differ in reduction potential (eq. 3.6-3.8). Pd^{2+} ion which higher reduction potential than Fe^{2+} will be reduced while Fe^0 atom will be reduced. Pd atoms are continuously generated after reducing and growth on the surface of iron. The general mechanism of palladium reduction can be represented by the following equation34.6-3.8 (Wang et al., 2009).

$$Pd^{2+} + Fe^0 \rightarrow Pd^0 + Fe^{2+} \quad (3.6)$$

$$Pd^{2+} + 2e^- \rightarrow Pd^0 \qquad E^0 = 0.987\ V \quad (3.7)$$

$$Fe^{3+} + 3e^- \rightarrow Fe^0 \qquad E^0 = -0.04\ V \quad (3.8)$$

This work, palladization was performed in aqueous solution and used Pd nitrate as metal precursor. While most of the literatures Fe was charged into ethanol solution of palladium acetate (Chen et al., 2011). Different in metal ion precursor and medium may result to different in Pd dispersion on Fe particles.

An example SEM image of Pd modified CMC-stabilized Fe^0 bimetallic nanoparticles are shown in Fig. 3.25.

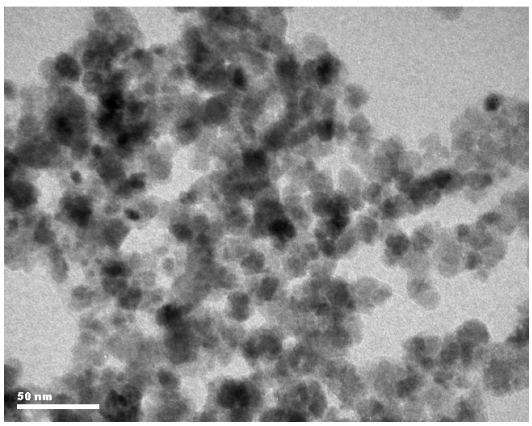

Figure 3.25 TEM image Pd modified CMC-stabilized Fe^0 bimetallic naoparticles prepared by palladization method. The reaction was carried out at at room temperature for 10 h, the

concentration of Fe^{3+} ion was 0.01 M. The mole ratio of Fe^{3+} to CMC was 1:5 ratios. The percentage of Pd loading was 0.2%.

From the image in Fig.3.26, there was no different in contrast between Pd and Fe particle observed. However, it can be noticed that the obtained particles after reduction of Pd over iron has clear boundary than unmodified Fe samples. It is possible that the modified sample prepared by palladization method providing an indication of the core/shell structure. However, it is difficult to confirm due to very low loading of Pd.

3.4.2 Preparation of Pd Colloidal Nanoparticles

Pd nanoparticles were prepared in colloidal form using polyol process. This method, metal salts should soluble in polyol solvent such as ethylene glycol which acts as a solvent for the metal salts, as well as a reducing agent, and a growth medium for the metallic products. This work, Pd colloidal nanoparticles were prepared by following the literature of Tedsree et al., 2011. $Pd(NO_3)_2$ was used as Pd^{2+} precursor, ethylene glycol was used as both polyol solvent and reducing agent and polyvinyl(pyrrolidone) (PVP) was used as stabilizer to prevent Pd nanoparticles from aggregation. Particle size, shape and distribution of the obtained PVP-Pd nanoparticles were characterized by transmission electron microscope. TEM images are shown in Figure 3.26.

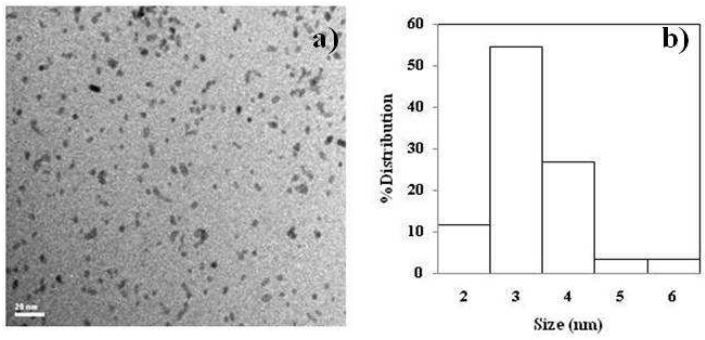

Figure 3.26 a) TEM images of Pd colloidal nanoparticles b) particle size distribution histogram.

From the image in Fig. 3.27, the obtained Pd particles display nearly spherical in shape with the average particle size 3.5±0.7 nm.

3.4.3 Nano-Palladium Deposition

This preparation method, both monometallic Fe^0 nanoparticles and Pd^0 nanoparticles were separately synthesized and redispersed in water in colloidal suspension. After mixing of the both suspension and stirring for 1h, the obtained Pd/Fe^0 colloidal nanoparticles were separated from the solution by centrifugation and wash with ethanol.The obtained samples was characterized by TEM, the images are shown in Fig. 3.27.

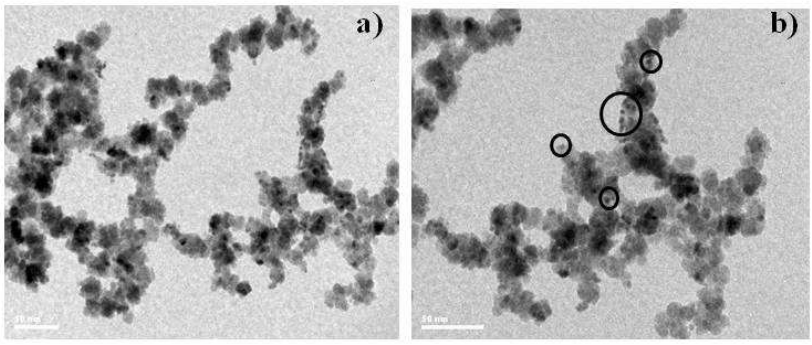

Figure 3.27 TEM images of Pd stabilized CMC-Fe^0 nanoparticles prepared by nano-palladium deposition method; a) low magnification b) high magnification. Pd nanoparticles are shown in the circle. CMC-Fe nanoparticle was synthesized at room temperature. The concentration of Fe^{3+} ion was 0.01 M. Mole ratio of Fe^{3+} to CMC was 1:5 ratios. Reaction time was 10 h and the percentage of Pd loading was 0.2.

From the images in Fig. 3.27, smaller spots which darker in contrast were observed. These spots were assigned to the particles of Pd metals. It is difficult to confirm that there is interaction between Fe and Pd particles and bimetallic particles were formed or both particles formed separately in monometallic particles. However, it seems likely that there is interaction between Pd and Fe particles due to no Pd particles dispersion outside Fe particles were observed from the images. In addition, due to strong metal-metal interaction, it is more likely that mixing of both monometallic Pd and Fe causing an interaction between Fe and Pd. The model of the obtained Pd/Fe bimetallic nanoparticles was proposed a shown in Fig. 3.29 a. While the island surface structure of the sample prepared by palladization was proposed in Figure 4.28 b)

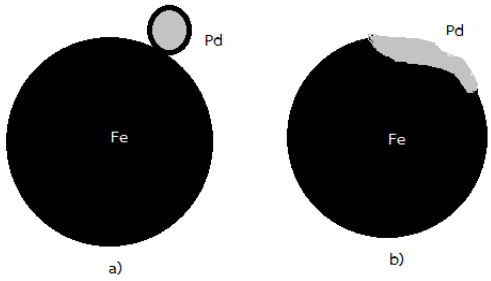

Figure 3.28 possible interactions of Pd and Fe in Pd/CMC-Fe nanoparticle prepared by a) nano-palladium deposition b) palladization.

TEM Images of the Synthesized Pd Modified Zero Valent Iron Nanoaprticles

TEM images of various % mole Pd modified zero valent iron nanoaprticles (analysis by EDX) prepared by various stabilizers and support materials are shown in Fig. 3.29-3.31.

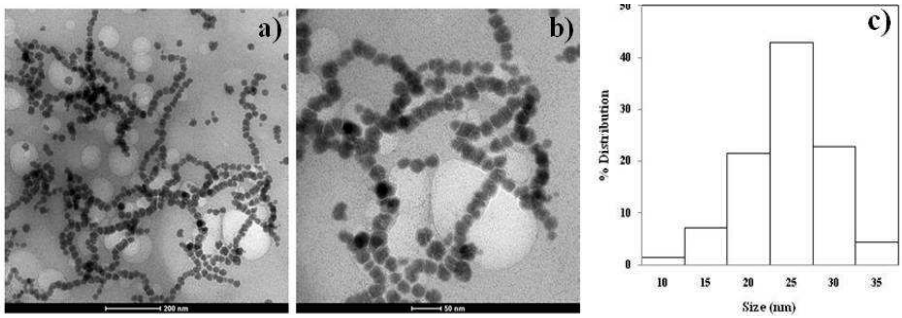

Figure 3.29 TEM images of Pd modified STR-Fe nanoparticles prepared by nano-palladium deposition method recorded a) at low magnification b) high magnification c) histogram of particle size distribution.

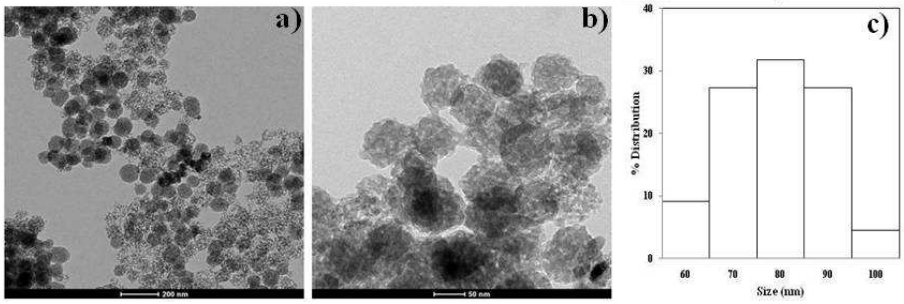

Figure 3.30 TEM images of Pd modified Fe nanoparticles on SiO_2 support prepared by nano-palladium deposition recorded a) at low magnification b) high magnification c) histogram of particle size distribution.

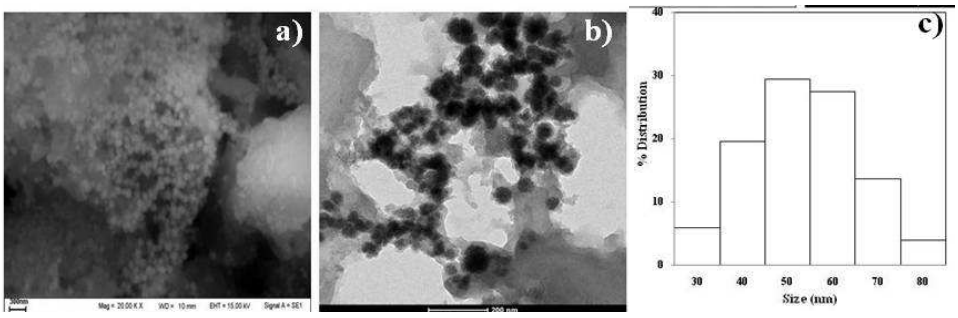

Figure 3.31 a) SEM image and b) TEM image of Pd modified Fe nanoparticles on carbon support prepared by nano-palladium deposition method c) histogram of particle size distribution

According to the images in Figure 3.30-3.32, it clearly showed that adding Pd nanoparticle on Fe nanoparticles by mixing both monometallic particles is not affect to the particle size and morphology of the Fe nanoparticles while the interaction between Pd nanoparticle and Fe nanoparticles was generated. Improving in their properties was expected.

3.5 Crystal Structure and Surface Compositions of the Synthesized Zero-valent Iron Nanoparticles

3.5.1 X-Ray powder diffraction (XRD)

X-Ray powder diffraction (XRD) was used to identify crystals structure of the synthesized zero-valent iron nanoparticles. XRD pattern of the synthesized CMC-Fe^0 measured at room temperature and 60 ºC are shown in Figure 4.32. The obtained XRD pattern reveals the existence of an amorphous phase of iron. For the sample prepared at 60◦C, an apparent peak at 35.80◦ to a characteristic peak of zero-valent iron (α-Fe) represent bcc (body-centered cubic crystal) Fe^0 lattice planes (110). For the sample prepared at room temperature, apparent peaks at the 2θ of 44.50° and 35.80° indicate the presence of both α-Fe and iron oxide (Fe_3O_4 and γ-Fe_2O_3) crystalline phases.

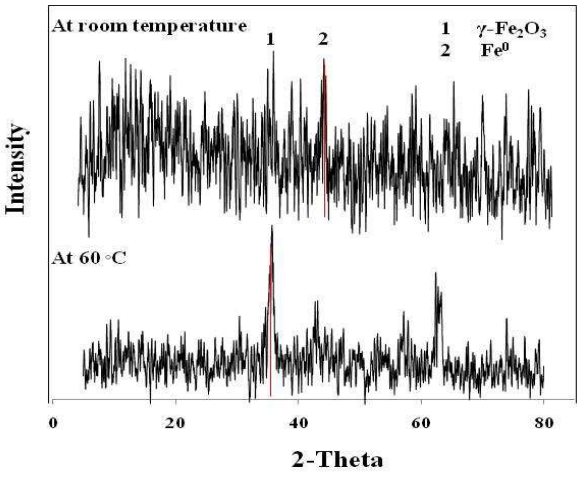

Figure 3.32 XRD patterns of the CMC-Fe nanoparticles prepared at room temperature and 60°C.

The results indicate that preparation of zero-valent iron nanoparticles at room temperature is less tend to generated oxide. It seems likely that preparation at high temperature is more suitable although it is very time-consuming and the particle size is larger

3.5.2 X-Ray Photoelectron Spectroscopy (XPS)

Important information about the surface molecular and electronic structure of the iron nanoparticles was provided by X-ray photoelectron spectroscopy. Wide scan or survey spectrum of CMC-Fe^0 nanoparticles is shown in Fig. 3.34.

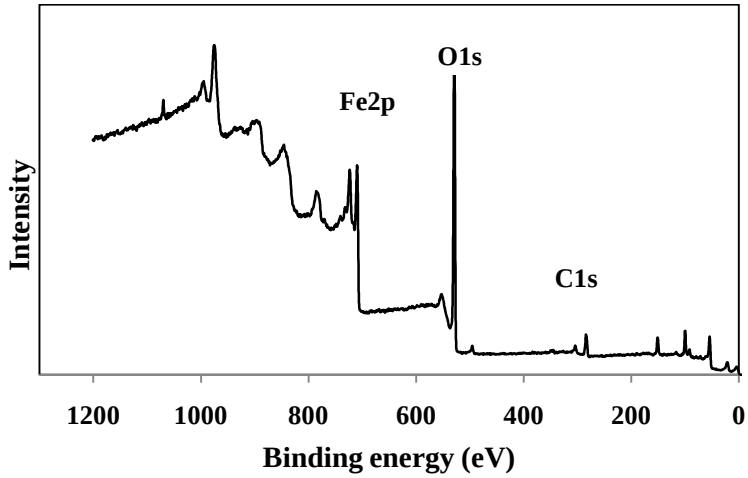

Figure 3.33 Wide scan XPS spectrum of the synthesized CMC-Fe^0 nanoparticles.

XPS spectra of Fe 2p, O1s and C1s of the synthesized CMC-Fe^0 nanoparticles are shown in Fig. 3.33. XPS spectra of Fe 2p, O1s and C1s of as synthesized CMC-Fe^0 nanoparticles are shown in Figure 3.34.

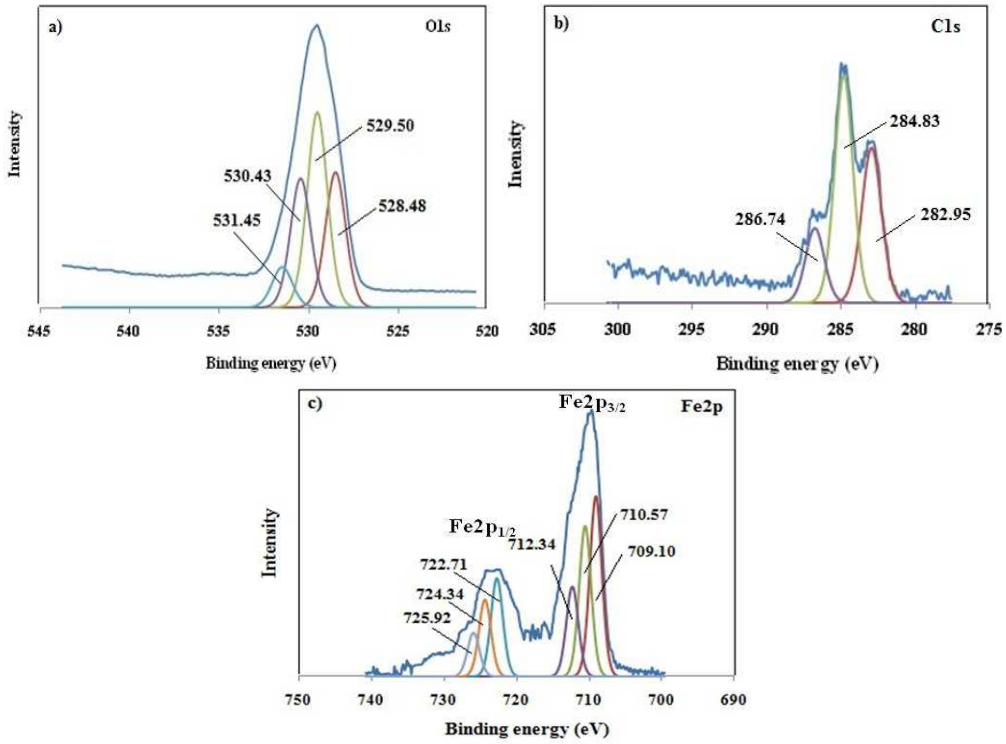

Figure 3.34 XPS spectra of a) O1s b) C1s and c) Fe 2p of the CMC-Fe^0 nanoparticles.

According to the spectra in Fig. 4.35a, the photoelectron peaks at around 709, 718, and 724 eV represent the binding energies of $Fe2p_{3/2}$, shake-up satellite $2p_{3/2}$, and $2p_{1/2}$, respectively (Sun et al., 2006). Curve-fitting analysis presented 2 oxidation states of iron components. By referring to the literatures, a peak at lowest binding energy (709.2 eV) corresponding to ferrous iron which may in form of surface hydroxide while a peak at higher energy (711.0 eV) suggests the presence of ferric iron. Fe^{2+} is the first form of surface oxidation in the presence of O_2 and water.

According to the spectra in Fig. 3.34b) The O1s decomposed into four peaks at 530.7, 531.7, 532.7 and 533.7 eV which peaks at binding energy 530.7, 531.7, and 533.7 eV corresponding to O^{2-}, OH, and chemically or physically adsorbed water, respectively (Sun et al., 2007) while the peak at 532.7 is characteristic of oxygen bonding to carbon which suggest the presence of oxygen of CMC coordinated on Fe nanoparticles (Nurmi et

al., 2012). The examination of the peak area ratios of OH^{-}/O^{2-} suggest that the oxide shell is composed of mainly iron hydroxides or iron oxyhydroxide; FeO(OH). The surface oxidation probably occurred during the sample transfer to the vacuum chamber for the XPS measurement (Guo et al., 2006). According to the spectra in Fig. 3.34c, the peaks at binding energy 282.9, 284.8 and 286.7eV are characteristic of the C-H, C-O and C=O, respectively (Sun et al., 2007).

4.5.3 Elemental Analysis of the Pd Modified Zero-valent Iron Nanoparticles

In order to confirm the elemental composition and elemental distribution of the obtained Pd modified zero-valent iron nanoparticles, energy-dispersive X-ray spectroscopy (EDX) was connected to scanning electron microscopy. This technique detects x-rays emitted from the sample during bombardment by an electron beam. The x-ray energy is characteristic of the element from which it was emitted. Thus, the elemental composition was determined. In addition, characteristic x-ray intensity can be measured relative to lateral position on the sample. Variations in x-ray intensity at any characteristic energy value indicate the relative concentration for the applicable element across the surface. The data of an elemental mapping was obtained.

EDX spectra of $Pd/Fe^{0}/SiO_2$ and $Pd/Fe^{0}/C$ nanoparticles are shown in Figure 3.35-3.36. The data of elemental compositions of all synthesized Fe^{0} nanoparticles are shown in Table 2.

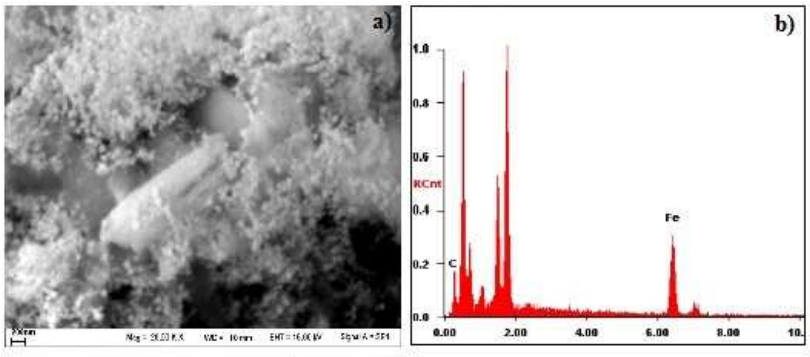

Figure 3.35 a) SEM image of $Pd/Fe^{0}/SiO_2$ nanoparticles b) EDX spectra

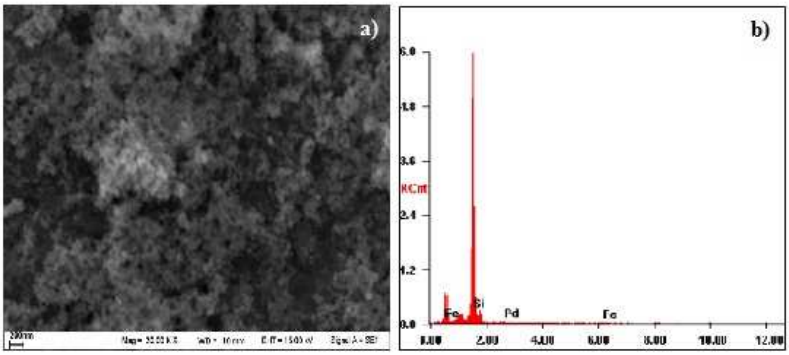

Figure 3.36 a) SEM image of Pd-Fe^0/C nanoparticles b) EDX spectra

Table 3.2 Elemental compositions of the synthesized zero-valent iron nanoparticles.

Fe^0 nanoparticles	Theoretical calculation				Elemental Analysis			
	Fe	Pd	Si	C	Fe	Pd	Si	C
Pd/CMC-Fe^0	99.90	0.1	-	-	99.00	1.00	-	-
Pd/CMC-Fe^0	99.80	0.2	-	-	98.92	1.02	-	-
Pd/CMC-Fe^0	99.70	0.3	-	-	98.33	1.67	-	-
Pd/CMC-Fe^0	99.60	0.4	-	-	98.51	1.49	-	-
Pd/CMC-Fe^0	99.50	0.5	-	-	98.02	1.98	-	-
Pd/STR-Fe^0	99.80	0.20	-	-	94.17	5.83	-	-
Fe^0/SiO_2	10	-	90	-	9.93	-	90.07	-
Pd/ Fe^0/SiO_2	10	0.20	89.80	-	10.17	2.98	86.85	-
Pd/Fe^0/C	20	0.20	79.80	79.48	19.81	0.36	-	79.83

According to the results in Table 3.2, it can be noticed that the elemental compositions of analyzed from EDX analysis are not close to the theoretical calculation. The reason of the error can be proposed in different cases. In case of using CMC as stabilizer, it is interesting that the obtained percentage of Fe contents for all samples are lower while Pd contents are higher than theoretical calculation. It is possible that there is leaching of Fe atoms due to oxidation reaction and washed out. In case of using starch as stabilizer, much lower in the percentage of Fe content obtained. It is possible that lost of Fe and gain of Pd resulting from incomplete reduction of Fe^{3+} to Fe^0 due to forming of Fe^{3+} hydroxide complexes in basic solution (pH 8). In comparison between CMC and starch stabilizer, CMC was strongly bond with Fe^{3+}at pH 8 and CMC-Fe^{3+} was fully reduced by $NaBH_4$ at room temperature while STR-Fe^{3+} stabilized by intra hydrogen bond. Thus, much different in Fe and Pd contents between calculation and preparation mainly

resulted from reduction process. In case of loading Fe in mesoporous pore of silica by wet impregnation. 20% of Fe content was loaded on mesoporous silica while excess amount of Fe^{3+} was washed out before reduction. It clearly showed that only about 10% of Fe could be load. In case of using carbon support, no problem of mass lost during the preparation, precipitation and separation method, thus the percentage of the elements is close to the theoretical.

3.6 Stability and Mobility of the Synthesized Zero-Valent Iron Nanoparticles

3.6.1 Dispersion Stability

Strong magnetic interaction between particles causes agglomeration which can limit colloidal stability and cause reduction of surface (Cook, 2009). This work, dispersion stability of the synthesized zero-valent iron nanoparticles were characterized in aqueous medium by visual inspection of settling behaviour (taking pictures at specific times to monitor the settling process). 0.01 g of the prepared iron nanoparticles was suspended in 10 mL of deoxygenated water and kept in close system. Dispersion stability of the zero-valent iron nanoparticles prepared with and without surface modification is shown in Fig. 3.37-3.38.

Initial time 25 min

Figure 3.37 Dispersion stability of zero-valent iron particles prepared without stabilizer.

Initial time after leaving for 7 days

Figure 3.38 Colloidal dispersion of the synthesized zero-valent iron nanoparticles a) STR-Fe^0 b) CMC-Fe^0 c) Fe^0/SiO_2 d) Fe^0/C nanoparticles compared between initial time and after leaving for 7 days. The concentration of Fe^0 nanoparticle is 1 g/L.

From Figure 3.37, bare iron nanoparticles which prepared without stabilizer settled to the bottom in less than 30 min while iron nanoparticles prepared in the presence of stabilizer or support materials remain suspend over a longer time. (Fig 3.38) After leaving for 7 days, STR-Fe^0 nanoparticles complete settled at the bottom while Fe^0/SiO_2 sample started to aggregate and settle out of the aqueous medium while CMC-Fe^0 nanoparticles and Fe/C nanoparticles remain in colloidal form with no noticeable of sedimentation or floccation. These suggest the formation of stable Fe^0 nanoparticle stable.

The dispersion stability of CMC-Fe^0 nanoparticles compare to Fe/C nanoparticles was further studied for 1 month; the results are shown in Figure 3.39

a) CMC-Fe^0 nanoparticles b) Fe^0/C nanoparticles

Figure 3.39 Dispersion stability of a) CMC-stabilized zero-valent iron nanoparticles b) carbon supported zero-valent iron nanoparticles form at different recorded time; initial time, after leaving for 15 days and 30 days.

Figure 3.39 a) the prepared CMC-stabilized zero-valent iron nanoparticles remains in suspension over an extended period of time (> 1 months) with no noticeable sedimentation or flocculation. The results indicate that both electrostatic and steric hindrances of CMC are very important in the stabilization. The improvement of

nanoparticle stability is due to strong complexation of Fe^{3+} precursor with the carboxylate groups of CMC in basic solution. Complexation of these ions during the reduction process does not only prevent nanoparticles growth to large size but also promote CMC strong attachment to the iron nanoparticle surfaces, which prevents particle agglomeration. Fe/C nanoparticles has lower dispersion stability in comparison with CMC-Fe nanoparticles. It can remain in colloidal suspension less than 15 days. Therefore, the order of colloidal stability was CMC-Fe nanoparticles > Fe^0/C nanoparticles > Fe/SiO_2 nanoparticles > STR-Fe^0 nanoparticles.

3.6.2 Mobility

A critical issue for the future development of *in situ* remediation technology involves zero-valent iron nanoparticles is delivery of the treatment to the contamination in the subsurface environment (Carroll et al., 2013). Zero-valent iron nanoparticles should be able to transport through the soils while maintaining adequate reactivity with the target contaminants under subsurface conditions. There is a little information available on the transport of zero-valent iron nanoparticles. In laboratory soil column experiments, the mobility of pure iron nanoparticles showed limitation due to the colloidal nature. Data from some recent field tests indicate that the iron nanoparticles may migrate only a few inches to a few feet from the point of injection (Li et al., 2006).

This work, the mobility of all synthesized zero-valent iron nanoparticles was preliminary test in laboratory by sand column experiment. Photographs showing sand column and the mobility of CMC-stabilized zero-valent iron nanoparticles through the column of sand are shown in Fig. 4.40a-d.

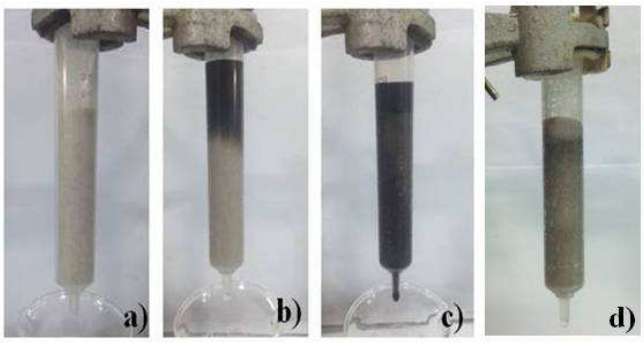

Figure 3.40 Photographs showing mobility of CMC-stabilized zero-valent iron nanoparticles through sand column recorded at a) 0 s, b) 10 s and c) 20 d) 30 s.

From Fig 3.40, it can be seen that all of the colloidal samples passed through the column in 30 min. Approximately 10 mL of deionized water was allowed to pass through the sand bed to elude the suspension. Most of the particles were able to pass through while only a small amount of particles remained on top of the sand bed. It is imply that the CMC-stabilized zero-valent iron nanoparticles have high mobility to transport in soil. The mobility of other synthesized zero-valent iron nanoparticles was also examined. Bare Fe nanoparticles cannot pass though the sand column, only clear aqueous solution passed through the porous of sand and most of the particles were observed to accumulate on the top of the sand column. Adding stabilizer or support clearly showed enhanced in their mobility. The colloidal dispersion of CMC-Fe and Fe^0/C nanoparticles can fully pass through the column. The results suggested that the anionic surface charges of CMC stabilizer and carbon support materials on the surface modified iron samples can enhance its transport whereas bare iron nanoparticles aggregate and impede the flow of water through the column. In case of STR-Fe^0 and Fe^0/SiO_2, some of the colloidal suspension can move along the column but only clear solution passed through the column. The results from stability and mobility test clearly demonstated that CMC-Fe nanoparticles and Fe/C nanoparticles are suitable for in-situ remediation of contaminant groundwater.

3.6.3 Particle Size and Zeta Potential Analysis

Particle size of nanoparticles can also be determined by dynamic light scattering (DLS) technique, which utilized the random changes in the intensity of light scattered from a suspension. This technique, the particle size diameter was reported in term of hydrodynamic diameter which contains of protecting layer of stabilizer. In addition, in order to confirm the potential stability of the synthesized zero-valent iron nanoparicles, zeta (ζ) potential was analysis. This work zeta potential was measured in an aqueous medium at pH 7. The results from dynamic light scattering and zeta potential are shown in Table 3.3.

Table 3.3 Zeta potential analysis of the colloidal dispersion of zero-valent iron nanopartilces.

Samples	Hydrodynamic	Zeta	Polydisper-	Mobility	Conductivity
CMC-Fe^0	696±2.5	35.7±1.0	0.39±0.2	-2.50±0.1	0.04
STR-Fe^0	1053±13.1	-16.3±1.1	0.45±0.1	-0.87±0.1	0.48
Fe^0/SiO_2	1054±27.9	-20.6±0.4	0.78	-1.62±0.2	0.13
Fe^0/C	706±2.2	-37.2±2.4	0.33±0.1	-2.92±0.2	0.02
Pd/CMC-Fe^0	447±5.0	-42.5±1.6	0.52	-3.34±0.1	0.02
Pd/STR-Fe^0	4196±148.3	-21.87±1.2	1	-1.71±0.1	0.5
Pd/Fe^0/SiO_2	1332±40.5	-26.36±0.5	0.48±0.1	-2.07±0.1	0.11
Pd/Fe^0/C	856±4.5	-32.80±0.7	0.35±0.2	-3.20±0.1	0.01

The particle size determined by TEM compared with DLS technique, hydrodynamic sizes of the synthesized Fe^0 nanoparticles analyzed by DLS are larger. The main differences between the measured diameters from these two techniques are due to the presence of an adsorbing layer on the surface of the particles.

Zeta potential is the potential difference between the dispersion medium and the stationary layer of fluid attached to the dispersed particle. A high zeta potential will confer stability, dispersion will resist aggregation. When the zeta potential is low, attraction exceeds repulsion and the dispersion will break and flocculate while high zeta potential (negative or positive than 30 mV) are electrically stabilized while colloids with low zeta potentials tend to coagulate or flocculate. From table 3.3, it can be seen that using CMC and activated carbon to prevent aggregation of iron nanoparticles, the obtained CMC-Fe^0 nanoparticles and Fe^0/C nanoparticles showed zeta potential value more negative than 30 mV which considered as stable colloids. While using starch as stabilizer and SiO_2 support, the zeta potential of the obtained STR-Fe^0, Pd/STR-Fe^0, Fe^0/SiO_2 and Pd/Fe^0/SiO_2 is less negative than 30 mV which considered as unstable colloidal particles. It means that these particles are unstable and can become immobile in an aqueous solution. These particles may adhere to negatively charged minerals or natural organic matter surfaces before reaching target contaminants (Cirtiu et al., 2011).

Polydispersity index (PDI) is the square of the standard deviation / mean diameter**.** It is related to the colloidal stability and should be less than 0.3. Samples with very broad size distribution have polydispersity index values > 0.7. If the PDI value is equal and/or greater than 1, the solution occur visual precipitation (nano.indiana.edu/Zetasizer_faq., 2015). From table 3.3, the PDI of the synthesized Fe^0 nanoparticles was found ranging from 0.3 to 1.0 that reflecting agglomeration of the particles. It can be noticed that the average hydrodynamic radius and polydispersity index increases in the case of Pd modified Fe^0 samples**.** In addition, a direct correlation existing between zeta potential, particle size and polydisersity index was found. Higher negative zeta potential, Fe^0 nanoparticles are smaller in size with low polydispersity index. Smaller size of the particles, the mobility of particles increases while conductivity of the particles decreases. These results are consistent with preliminary test, CMC-Fe^0 nanoparticles and Fe^0/C nanoparticles. CMC-Fe^0 and Fe^0/C nanoparticles showed high-ability materials to use in *in situ* remediation technology.

Section II Dechlorination of 1,2 Dichloroethane

3.7 GC analysis of 1,2 Dichloroethane

Volatile organic compound analysis is typically done by either purge and trap (P&T) or headspace (HS) technique (Barani et al., 2006). This work, head space–solid-phase microextraction (HS-SPME) and gas chromatography were used for the determination of 1,2 dichloroethane contaminant in water.

3.7.1 Head Space Solid Phase Microextraction

The HS-SPME is an equilibrium process of analysts between the vapor phase and fiber coating. In order to optimized HS-SPME conditions, the extraction parameters such as extraction time, magnetic stirring, the volume ratio of sample to headspace, extraction temperature and desorption time were investigated.

Effect of Extraction Conditions

Typically, SPME is considered complete when the analytes concentration has reached distribution equilibrium between the sample matrix and the fiber coating. Thus

it is important to determine the time that analytes reach equilibrium. This work, polydimethylsiloxane (PDMS) was used as SPME fiber coating. In order to evaluate the extraction efficiency, extraction times, headspace volume, magnetic stirring and desorption time was studied. Different extraction times from 1 to 10 min were examined. The temperature was studied at 23°C. The relationship between extraction time and analyte absorbed on the fiber is shown in Figure 3.41.

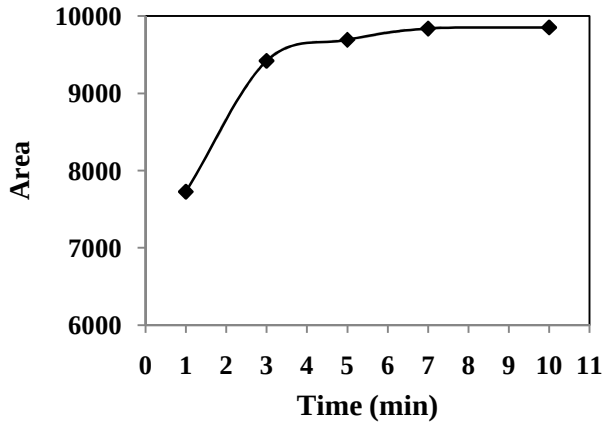

Figure 3.41 Effect of time on 1,2 dichloroethane extraction.

The optimal time for the extraction was achieved at 7 min which was the time of equilibrium between analyst and the polymeric phase of the fiber. As the volume of the gaseous phase in the HS-SPME should be minimized for higher recoveries according to the SPME theory, the ratio of sample to headspace volume was studied. The best result was obtained at 10/10 mL volume ratio of sample to headspace. In addition, stirring rate was found affected to extraction efficiency, because stirring can speed up the transfer of the compounds from water to headspace. From the studied, the best recoveries for all compounds were observed at 1000 rpm. Desorption time was also studied. The results showed that all compounds were completely desorbed at 7 min at 200 °C.

3.7.2 Determination of 1,2 Dichloroethane by Gas Chromatagraphy

The amount of 1,2 dichloroethane was analyzed on a Hewlett Packard HP 5890 series II gas chromatograph with FID detector. Separation of the 1,2 dichloroethane was obtained on a HP-5MS UI column (30 m × 0.32 mm i.d., 0.25 μm film) using helium as carrier gas (flow-rate, 3 ml/min). The GC conditions were; column temperature 90◦C,

injector temperature 200°C; detector temperature 250°C. The obtained GC spectrum of 1,2 dichloroethane is shown in Fig. 3.42

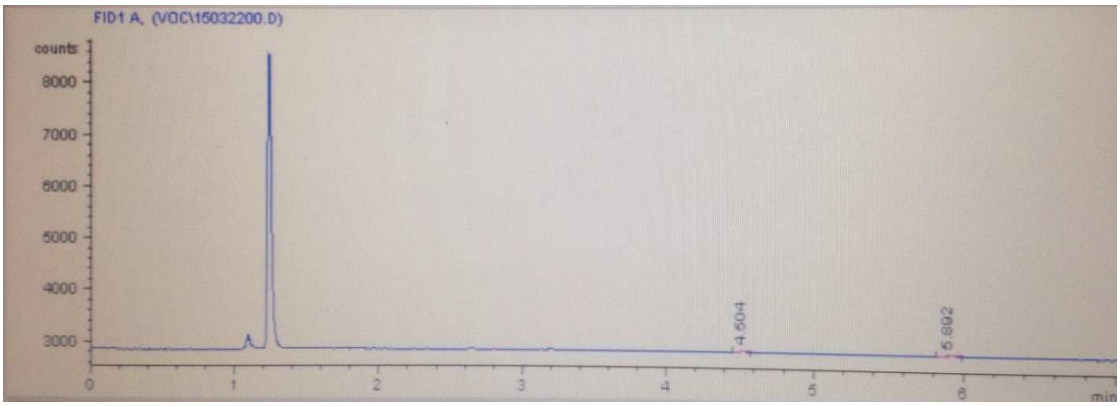

Figure 3.42 GC spectrum of 1,2 dichloroethane.

From the chromatogram, a peak at retention time 1.23 is assigned to 1,2 dichloroethane while the small peak at 1.07 is assigned to methanol contaminant from stock solution.

To ensure optimization of the methods in light of the standardization rules, the developed methods were validated in terms of linearity, precision, accuracy, LOD, LOQ. Five calibration solutions in the range 1 -5 ppm were prepared by suitable dilution of water. Linearity curve is plotted with peak areas against the concentration of 1,2 dichloroethane. The HS-SPME extraction was performed in triplicate. The relative area was plotted against the relative concentration as shown in Fig. 3.43.

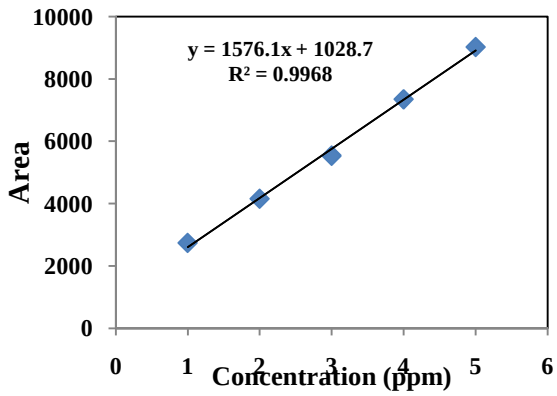

Figure 3.43 Calibration curve of 1,2 dichloroethane.

Linearity equation observed for 1, 2-dichloroethane is y = 1576.1x + 1028.7. The correlation coefficient values observed is 0.9968 which is a good linearity in the tested concentration range. The limit of detection was determined using a 3SD/slope ratio and the limit of quantification using a 10 SD/slope, where SD is the standard deviation of the mean value of fortified blank at 0.001 ppm. LOD and LOQ were 0.06 ppm and 0.2 ppm respectively. 10 samples of 5 ppm of 1,2 dichloroethane were analyzed on the day tested, the % RSD was found less than 5.0%, and accuracy (relative error) was better than 1.5%

3.8 Dechlorination of 1,2-Dichloroethane Contaminant in Water

This work, catalytic performance of the synthesized Fe^0 nanoparticles and Pd/Fe^0 bimetallic nanoparticles towards dechlorination of 1,2 dichloroethane contaminant in water was investigated in laboratory scale. The samples were prepared in 20 mL headspace vial by spiking aqueous solution of 1,2 dichloroethane in deoxygenated distillated water which contained Fe^0 colloidal nanoparticles. The solution was filled without a headspace. The vial was rolled on the roller bottle at room temperature for desired time. The control samples were prepared by the same process but the catalyst was not added. Dechlorination efficiency was reported in term of relative concentration of final concentration and initial concentration (C/C_0) and also reported on the percentage of dechlorination.

3.8.1 Dechorination Efficiency of 1,2-dichloroethane by CMC-Fe^0Nanoparticles

The catalytic performance of CMC-stabilized Fe^0 nanoparticles toward dechlorination of 1,2 dichloroethane was investigated in an aqueous colloidal dispersion. As, dechlorination reaction happens on the surface of catalyst thus the degradation process requires many steps; a) movement of 1,2 dichloroethane from the solution to the surface of the Fe particles; b) adsorption on the surface c) reductive dechlorination on the surface d) desorption of the reduced products from the surface and e) transfer products to the bulk solution (Reddy et al., 2010). Therefore, there are many factors affected to the degradation efficiency. This work, the effects of an initial concentration of 1,2 dichloromethane and the ratio of catalyst to solution were studied.

Effect of Initial Concentration of 1,2 Dichloroethane

The initial concentration of substrate plays an important role in degradation process. This work, the effect of concentration on the dechlorination efficiency of 1,2 dichloroethane by CMC-Fe^0 nanoparticles was studied at 1 and 5 ppm. The particle size of CMC-Fe^0 nanoparticles was 45±6 nm. The reaction time was varied in range 1 to 24 hr. The results are shown in Figure 3.44.

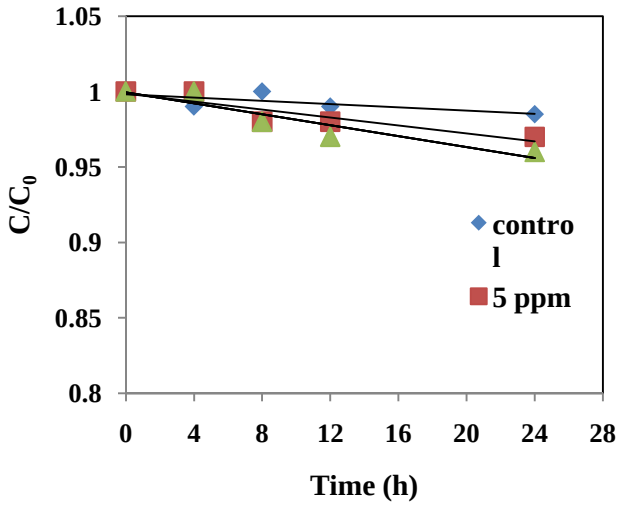

Figure 3.44 the effect of initial concentration of 1, 2 dichloroethane on the relative concentration of 1, 2 dichloroethane at different reaction times. The ratio of catalyst to solution was 1 g/L.

According to the graph in Fig. 3.44, it is demonstrated that there is only a little change in the concentration of 1,2 dichloroethane compared to the control samples. Although the initial concentration concentration of 1,2 dichloroethane was decreased from 5 to 1 ppm. Only 4% dechlorination (C/C_0 = 0.946) was obtained at 24 h. In order to determine the maximum efficiency, further study should be carried out to determine the optimum conditions by varying reaction parameters affected to the catalytic efficiency.

Effect of Ratio of Catalyst to Solution

Degradation efficiency could increase with an increase amount of Fe^0 nanoparticles (Cho et al., 2010). An increase ratio of Fe^0 nanoparticles would be expected to increase the quantity of reactive Fe sites resulted in an enhance dechlorination efficiency. This work, the effect of catalyst addition on dechlorination of 1,2 dichloroethane was investigated. The amount of CMC-Fe^0 nanoparticles to solution was studied between 1-4 g/L. The

particle size of CMC-Fe^0 nanoparticles used for this testing was 45±6 nm.The results are shown in Figure 3.45.

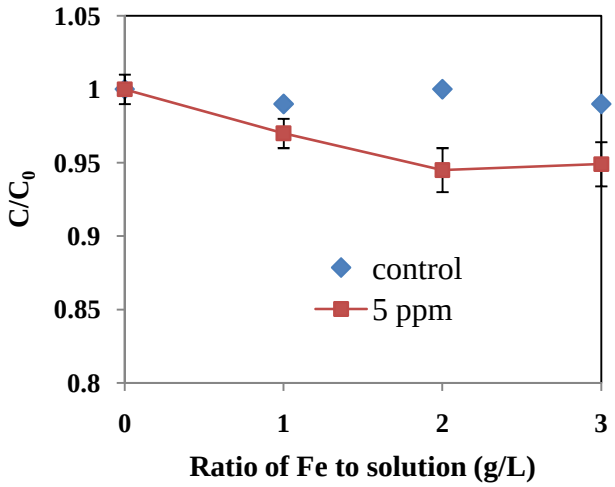

Figure 3.45 Effect of ratio of CMC-Fe^0 nanoparticles to solution to dechlorination efficiencies of 1,2 dichloroethane. Initial concentration of 1,2 dichloroethane was 5 ppm, Reaction time was 24 h.

The results from Fig 3.45 showed that the concentration of 1,2 dichloroethane slightly decreasese when the ratio of CMC/Fe^0 nanoparticles to solution was increased from 1 to 2 gFe/L. The maximum percentage of dechlorination was 5.5 (C/C_0 = 0.945). At higher concentration, the dechlorination efficiency tends to decreases. This showed that the dechlorination efficiency of 1,2 dichloroethane might not be increased unlimitedly with increasing the addition of CMC/Fe^0 nanoparticles. It is possible that high concentration of iron nanoparticles causes the particles tendency to agglomerate and aggregate resulting in severely limit of surface area. Moreover, high concentration of CMC stabilizer caused limitation of 1,2 dichloroethane transportation. At the ratio of Fe^0 nanoparticles to solution higher than 4, too viscous CMC stabilized Fe^0 nanoparticles were found due to limited space of vial. In addition, excessive hydrogen may suppressed the continuation of both corrosion of iron and reduction reaction of 1,2 dichloroethane by act as site blocker. These are major limiting factors for the occurrence of dechlorination in a small limited area rather than using in natural groundwater.

From the results, much lower in catalytic performance of Fe^0 nanoparticles toward 1,2 dichloroethane compare to other chlorinated alkane. Song and co-worker prepared nanosized iron particles (80-100 nm in diameter) and used it as catalysts for

dechlorination of 8 chlorinated ethanes; hexachloroethane (HCA), pentachloroethane (PCA), 1,1,2,2-tetrachloroethane (1,1,2,2-TeCA), 1,1,1,2-tetrachloroethane (1,1,1,2-TeCA), 1,1,2-trichloroethane (1,1,2-TCA), 1,1,1-trichloroethane (1,1,1-TCA), 1,2-dichloroethane (1,2-DCA), and 1,1-dichloroethane (1,1-DCA)) in batch reactors. The results showed that all chlorinated ethanes except 1,2-dichloroethane were transformed to chlorinated ethanes or ethenes (Song, and Carrway, 2005). The results was clearly confirmed the high structural stability of 1,2 dichloroethane. It is possible that the particle sizes of Fe^0 nanoparticles used in this work (45 nm) and the above report (80-100 nm) are too large. Thus, the effect of particle size of Fe catalyst on the dechlorination efficiency was further explored.

Effect of the Particle Size of Fe^0 Nanoparticles

Decreasing the particle size, increasing the amount of an active surface sites and enhancing the catalytic properties were expected. Two different particle sizes of CMC-Fe^0 nanoparticles were prepared at different ratios of Fe to CMC stabilizer. The 45 nm of CMC-Fe^0 sample was prepared with 1:5 ratio for 10 h. while the sample with 12 nm diameter was prepared at 1:10 Fe to CMC ratio for 6 h. The effect of particle sizes of CMC-Fe^0 nanoparticles toward dechlorination of 1,2 dichloroethane was studied. The results are shown in Figure 3.46

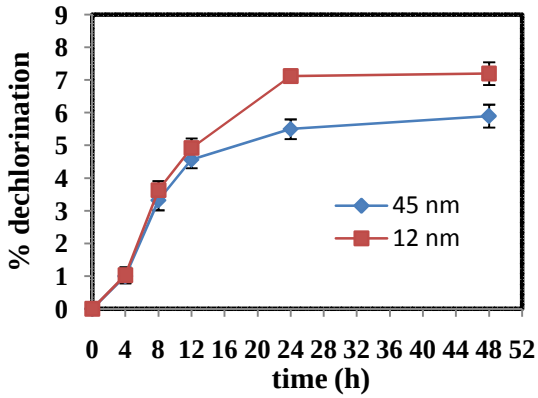

Figure 3.46 Effect of particle size of CMC-Fe^0 nanoparticles on the dechlorination efficiency of 1, 2 dichloroethane. The ratio of catalyst to solution was 2 gFe/L.

Decreasing of the particle size of CMC-Fe^0 nanoparticles from 45 to 12 nm, enhance in catalytic activity was obtained. It demonstrated that the activity of iron nanoparticles depends on their particle size. Thus, smaller in size of Fe^0 nanoparticles with high surface area is required. However, only about 2% dechlorination increasing after was

obtained from this experiment. In addition, it is noticed that there is continuously increase in % dechlorination at first day while a little change was obtained in the next day. It may be caused by catalyst deactivation.

3.8.2 Reaction Mechanism of Dechlorination of 1,2 Dichloroethane by Fe^0 Nanoparticles

In the process with containing Fe^0 nanoparticles in water, the chemical reaction is shown in Eq 3.9.

$$Fe + 2H_2O \rightarrow Fe^{2+} + H_2 + 2OH^- \quad (3.9)$$

Fe and Fe^{2+} species play a role in reductive dechlorination of chlorinated hydrocarbon. In case of the reaction contain O_2 in water, Fe^{2+} and Fe^{2+} species are formed on the surface as shown in Eq 3.10.

$$2Fe + O_2 + 2H_2O \rightarrow 2Fe^{2+} + 4OH^- \quad (3.10)$$

Fe^{2+} can be further oxidized to Fe^{3+}:

$$4Fe^{2+} + 4H^+ + O_2 \rightarrow 4Fe^{3+} + 2H_2O \quad (3.11)$$

Fe^{3+} reacts with OH^- or H_2O and to yield hydroxide or oxyhydroxide:

$$Fe^{3+} + 3OH^- \rightarrow Fe(OH)_3 \quad (3.12)$$

$$Fe^{3+} + 2H_2O \rightarrow FeOOH + 3H^+ \quad (3.13)$$

$Fe(OH)_3$ can also dehydrate to form FeOOH:

$$Fe(OH)_3 + 3H^+ \rightarrow FeOOH + H_2O \quad (3.14)$$

The reductive dechorination of 1,2 dichloroethane may involve either direct or indirect reduction or both. Direct reduction, dechlorination of 1,2 dichloroethane processes by direct reduction at Fe atom on the surface of Fe^0 nanoparticles. While indirect reaction, dechlorination reduction by ferrous ion involved reduction of water by Fe atom. Fe^{2+} species generated from oxidation reaction by water further reacted with 1,2 dichloroethane. The reaction pathways are shown in Fig. 3.47.

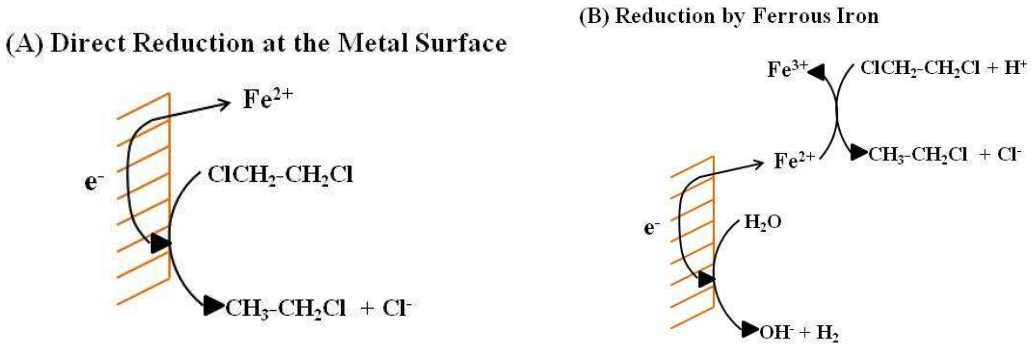

Figure 3.47 Possible dechlorination pathways of 1,2 dichloroethane by CMC- Fe^0 nanoparticles.

From both pathways, it can be seen that there is competition between water and 1,2 dichloethane for adsorption on the surface of Fe^0 nanoparticles. Reduction of water is more likely to occur than 1,2 dichloroethane which contaminated in water at low concentration. Thus, the dechlorination process by direct reduction on Fe^0 atom of the surface is less opportunity. The reduction by ferrous ion seems to play more important role than direct reduction. As reduction potential of ferrous ion is not strong as Fe^0, dechlorination of 1,2 dichloroethane (highly stable molecule) may not degrade via this process. One possible way to increase the performance of Fe^0 is decreasing their particle sizes. Due to it is not only increase surface area and active sites but also change their electronic properties affected to absorption and dechlorination ability. It is possible that decreasing the particle size resulted in strongly active sites of Fe for adsorption and decompose of 1,2 dichloroethane. The dechlorination reaction processed via direct reaction.

From reduction by ferrous ion pathway, H_2 gas was generated, thus another way to use H_2 as reducing agent is making it adsorption on metal surface. An increase rate of dechlorination of 1,2 dichloroethane by using bimettalic Fe^0 nanoparticles will be further explored.

3.8.3 Dechlorination of 1,2-dichloroethane by Bimetallic Pd-modified Fe^0 Nanocatalyst

Palladium is known as a good catalyst for hydrogenation reactions (Cho et al., 2010). Pd modified Fe nanoparticle has been accepted as high performance catalyst for dechlorination reduction of chlorinated hydrocarbon (Wang et al., 2009). This work, the catalytic efficiency of Pd modified Fe nanoparticles toward dechlorination reaction of 1,2 dichloroethane will be investigated. Important parameters such as surface structure of bimetallic and the effect of Pd loading was studied.

Effect of Surface Structure of Bimetalic Catalyst on the Dechlorination Efficiency

Different preparation methods of bimetallic catalyst resulted in the difference of surface structure and compositions. This work, the effect of Pd modification method on the catalytic activity of bimetallic Pd/Fe^0 nanoparticles was studied. The catalytic performance of Pd/Fe^0 nanoparticles synthesized by palladization and nano-palladium deposition toward dechlorination of 1,2 dichloroethane were explored. The results are shown in Fig. 3.48.

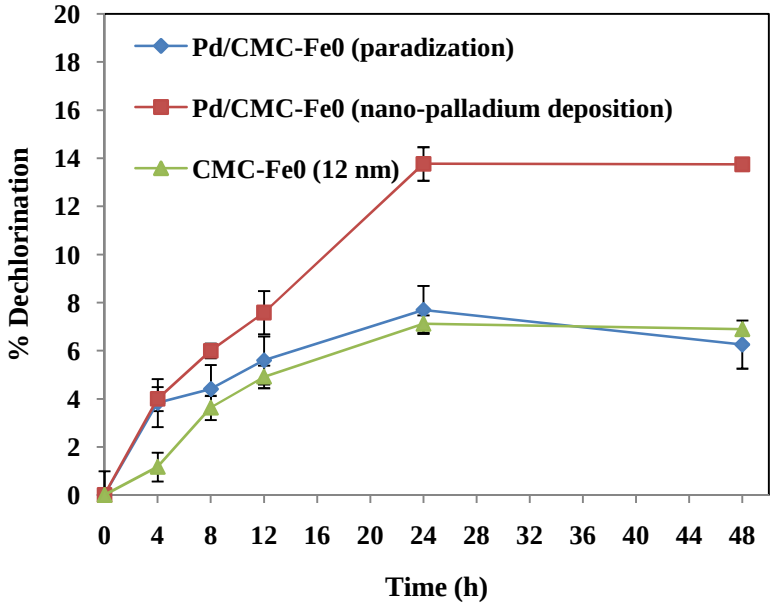

Figure 3.48 The effect of Pd modification method on dechlorination efficiency of 1,2 dichloroethane. Initial concentration of 1,2 dichloroethaane was 5 ppm. Catalyst to solution ratio was 2 g/L. %Pd loading was 0.2%.

By adding Pd on Fe^0 nanoparticles, the dechlorination efficiency was significantly increased. Rate of dechlorination of CMC-Pd/Fe^0 nanoparticles is much higher than CMC-Fe nanoparticles at first 4 h. It means Pd, as catalyst, plays, an important role in this reaction. The CMC stabilized Pd/Fe^0 nanoparticles prepared by nano-palladium deposition exhibited nearly two times greater reactivity toward dechlorination of 1,2 dichloroethane than the Pd/Fe^0 nanoparticles prepared by palladization. There are numerous literature studied on the dechlorination of chlorinated hydrocarbon by using Pd/Fe bimetallic nanoparticles prepared by palladization method (Sakulchaicharoen et al., 2010). Their high performance catalytic activity for dechlorination was confirmed for almost chlorinated hydrocarbon. Some reports studied on dechlorination of chlorinated hydrocarbon by using the mixture of monometallic Pd and Fe particles as catalyst. From the report of Zhang and co-worker, the Pd and Fe nanoparticles are separately added in the sample solution. The result was found no better than adding Fe alone. While doping Pd on the surface of Fe to form integrated bimetallic complexes (Pd/Fe), enhanced reactivity toward trichloroethane degradation was obtained (Zhang et al., 1998). However, He and co-worker reported on trichloroethane degradation that the mixture of CMC-stabilized monometallic Fe and Pd nanoparticles exhibited a nearly two times greater reactivity than the Fe-Pd bimetallic nanoparticles. For separately mixing, the highly reactive Fe^0 nanoparticles can undergo rapid corrosion reaction with water to give off H_2. Therefore, the observed highly effective degradation of trichloroethane is attributed to reduction by H_2 with the Pd nanoparticles as catalysts. For the bimetallic Fe-Pd nanoparticles, the presence of Pd on the Fe surface is expected to catalyze trichloroethane reduction by both Fe^0 and H_2. However, the slower overall trichloroethane degradation rate with the bimetallic nanoparticles indicates that the overall trichloroethane degradation rate is not limited by the Fe corrosion, but rather by the catalytic activity of Pd.

This work, Pd and Fe nanoparticles were firstly mixed in colloidal form and the product was centrifuged out. It is possible that there is physical interaction between Pd nanoparticle and Fe^0 nanoparticle at interface. When they are in contact, electron will transfer from Fe to Pd due to different in electronegativity resulting in higher electron density of Pd, enhanced adsorption and reduction ability of H_2 gas to hydrogen atom. For the sample prepared by palladization, the surface of Fe was covered by Pd atoms resulting in decrease of Fe active surface. In comparison with Pd particle deposited on Fe surface,

surface area of Fe is not covered as prepared by palladization. Thus higher in catalytic activity was obtained. It is confirmed that surface structure of bimetallic play an important role in catalytic activity.

3.8.4 Effect of Pd Loading on the activity of Pd/Fe^0 Nanocatalyst toward Dechlorination of 1,2 Dichloroethane

The dechlorination efficiency of Pd/Fe^0 bimetallic nanocatalysts depends on the percentage Pd loading on Fe^0 nanoparticles. Addition of Pd enables the dechlorination rate increasing rapidly, but cost of treatment also increased. Therefore, the lowest level of Pd loading that can be still effective to dechlorinate 1,2 dichloroethane is economically desired. This work, effect of Pd loading on the catalytic performance of Pd/Fe bimetallic nanoparticles toward dechlorination of 1,2 dichloroethane was explored. The relationship between % dechlorination and % Pd loading of the bimetallic samples prepared by palladization and nano-palladium deposition is shown in Fig. 3.49.

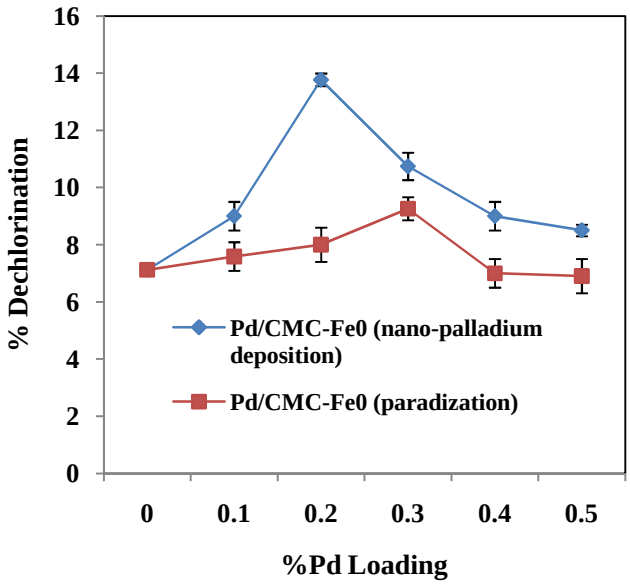

Figure 3.49 The effect of Pd loading on dechlorination efficiency of 1,2 dichloroethane with various percentage of Pd loading on Pd/CMC-Fe^0 bimetallic prepared by palladization and nano-palladium deposition. Initial concentration of 1,2 dichloroethaane was 5 ppm. Catalyst to solution ratio was 2 g/L.

For the Pd/CMC-Fe^0 nanoparticles prepared by nano-palladium deposition, the optimum catalytic efficiency is obtained at Pd loading (0.2%) while the sample prepared

by palladization, need higher Pd loading (0.3%). The maximum percentage of dchlorination reaction was 14%. Further increasing of Pd loading, the dechlorination activity become continuously decrease.

As the dechlorination of 1,2 dichloroethane occurs once they are adsorbed on the Pd/Fe surface, it is possible that increase Pd loading cause decreasing of Fe atom at the surface resulting in lower in catalytic activity. Pd on the surface of Fe particles plays the role of a collector of hydrogen gas that results from the oxidation of Fe particles. An increase in Pd content with bimetallic could promote the iron oxidation and consequently the rate and extent of dechlorination. A higher catalytic metal loading could increase the number of catalytic metal 'islands' on the iron surface. The increased amount of Pd coating on Fe^0 might hinder the formation of H_2 by Fe^0 corrosion. Dechlorination reaction depended on an active iron surface, and presumably the number of active sites on the surface was not large enough for effective dechlorination, thus the dechlorination efficiency decreased when Pd loading was more than 0.2 mole%. For colloidal mixing of Fe and Pd monometallic nanoparticles, the percentage of dechlorination increase with increasing the amount of Pd adding. The maximum activity was 14 percent dechlorination at 0.2% Pd loading. Further increase the amount Pd loading, percentage of dechlorination the decrease the same as Pd/Fe^0 catalyst prepared by palladization.

3.9 Dechlorination Efficiency of the Synthesized Catalysts

Degradation efficiency of the all synthesized Fe^0 nanoprticles and Pd/Fe bimetallic nanoparticles toward dechlorination of 1,2 dichloethane was explored and shown in Figure 4.51.

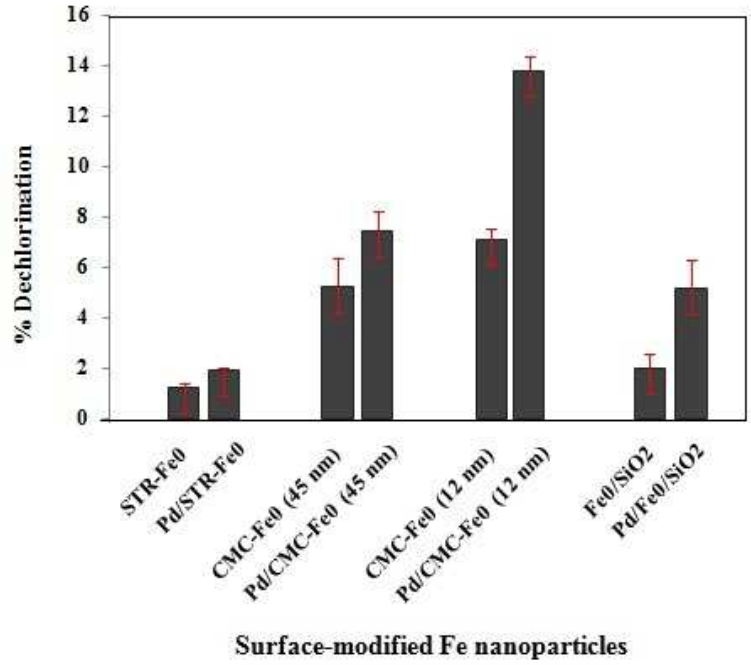

Figure 3.50 Dechlorination efficiency of Fe nanocatalysts and Pd/Fe bimetallic nanocatalysts prepared by different polymer stabilizer and support materials toward dechlorination of 1,2 dichloroethane. Concentration of catalyst was 2g/L, reaction time was 24 hour and initial concentration of 1,2 dichloroethane was 5 ppm, %Pd loading was 0.2% (w/w).

According to the results in Fig 3.50, it was clearly showed that modification of Fe nanoparticles with polymer stabilizers or support materials resulting in much increase in dechlorination efficiency. All of the synthesized Pd/Fe bimetallic nanocatalysts have much higher in the catalytic activity than monometallic catalysts. Pd/CMC-Fe^0 nanoparticles in comparison with CMC-Fe^0 nanoparticles, modified with Pd particles resulted in 2 times increase in dechlorination efficiency. The dechlorination activity reached 14% (12 nm of the Fe^0 samples). The catalytic dechlorination of 1,2 dichloethane are consistent with their colloidal dispersion stability and oxidation stability. Zero-valent iron nanoparticles coating by CMC showed the highest efficiency due to its high colloidal stability and oxidation stability to prevent formation of particle aggregates and high resistance particles to oxidation (long term using). In the case of using soluble starch as stabilizer, lower activity was obtained due to its low both dispersion and oxidation stability. It is prone to forming large particles by agglomeration, leading to a decline in its specific surface area and eventually reducing its dispersibility and reactivity. Due to the large surface area of Fe

nanoaparticles and the catalytic function of Pd, Pd/Fe bimetallic nanoparticles possess an effective dechlorination capability. Enhanced catalytic reaction was most likely ascribed to the ability of Pd to facilitate hydrogen adsorption and hydrodechlorination reaction.

In case of Fe^0/C nanoparticles which the results from characterization section showed high colloidal stability and oxidation stability, high catalytic activity toward dechlorination of 1,2 dichloethane was expected. However, HS-SPME techniques was found limited for extraction of 1,2 dichoroethane in water containing activated carbon due to electrolyte effect. The addition of an electrolyte in the sample matrix decreases the solubility of hydrophobic analytes in the aqueous phase. From the results, much increase in GC signal was detected compare to the control sample. This may cause from high negative charge of activated carbon contaminant increases volatile rate the 1,2 dichloroethane resulting in shifting the equilibrium toward the fiber.

3. 10 0Reaction Mechanism of Pd/Fe^0 Bimetallic Nanoparticles Toward Dechlorination of 1,2 Dichloroethane.

To identify intermediates and final products from dechlorination of 1,2 dichloroethane, the headspace gas generated from the dechlorination reaction was drew and identified by gas chromatography. HP 5 capillary column and FID detector was used. The column temperature is maintained at 80°C. Injector and detector temperature were set at 200°C. and 250°C, respectively. The flow rate was 1 mL/min. A Chromatogram of the headspace gas from generated from degradation of 1,2 dichloroethane is shown in Figure 3.51.

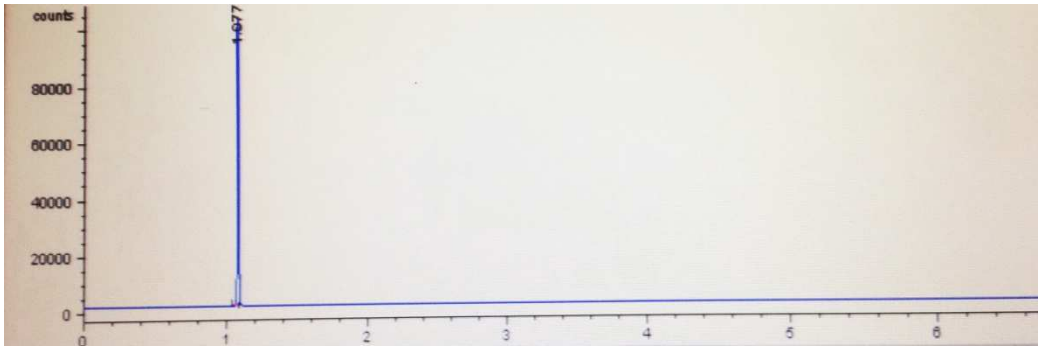

Figure 3.51 GC-FID chromatogram of headspace sample from degradation of 1,2 dichloroethane by Pd/CMC-Fe^0 nanoparticles.

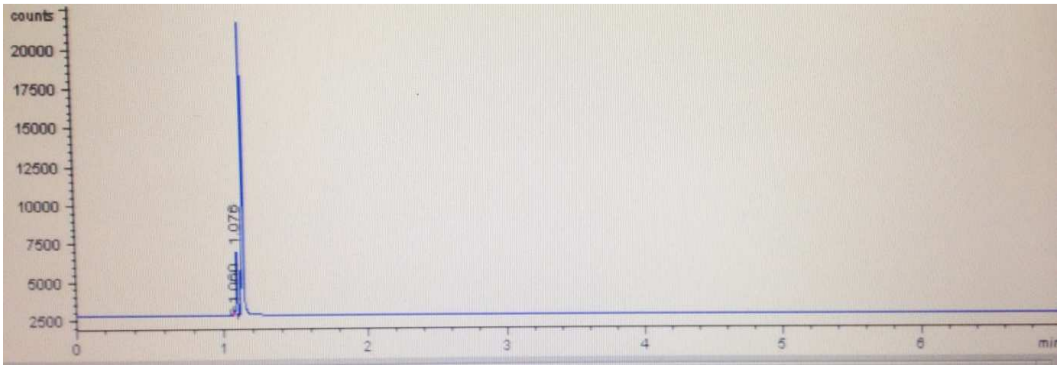

Figure 3.52 GC-FID chromatogram of standard ethane (ethane gas was obtained from electrolysis of acetic acid).

From Figure 3.51, In comparison to the standard of gas could be generated from the dechlorination reaction, a peak at retention time 1.07 is assigned to ethane. Typically, chloro group of 1,2-dichloroethane can be degraded into two reaction mechanisms; namely reductive dihaloelimination and hydrogenolysis. Dihaloelimination involves the removal of two halogen atoms that are adjacent on the same alkane molecule, leading to the formation of an additional carbon-carbon bond. 1,2-dichloroethane will be transformed to ethylene in single step (Eq.3.15). Hydrogenolysis or sequential degradation pathway is the replacement of the halogen atom with a hydrogen atom chloroethane (Eq.3.16) and ethane (Eq.3.17) in second step will be formed.

$$ClH_2C - CH_2Cl + 2e^- \rightarrow CH = CH + 2Cl^- \quad (3.15)$$

$$ClH\,C\text{-}CHCl + H^+ + 2e^- \rightarrow CH - CH\,Cl + Cl^- \quad (3.16)$$

$$HC\text{-}CHCl + H^+ + 2e^- \rightarrow CH - CH + Cl^- \quad (3.17)$$

From GC analysis, the main product from the reductive dechlorination of 1,2 dichloroethane was ethane. Therefore, it is indicated that the dechlorination follows hydrogenolysis reaction. The effectiveness of Pd/Fe bimetallic particles was most likely ascribed to the ability of Pd to facilitate hydrogen adsorption. The catalytic reduction of 1,2 dichloroethane by Pd/CMC-Fe^0 bimetallic nanocatalyst should followed these steps.: (I) the corrosion of iron leads to the emergence of H_2; (II) Pd and H_2 are combined to form a transitional compound Pd·H with H atom embedded in Pd crystal lattice; (III) Pd·H dechlorinates 1,2 dichloroethane. The reaction could be depicted by Eqs. (3.18) – (3.22). The schematic illustration of hydrodechlorination process is shown Figure 3.53.

$$Fe + 2H_2O \rightarrow Fe^{2+} + H_2 + 2OH^- \quad (3.18)$$

$$Pd + H_2 \rightarrow Pd \cdot H_2 \quad (3.19)$$

$$Pd + ClCH_2\text{-}CH_2Cl \rightarrow Pd \cdots Cl \cdots CH_2\text{-}CH_2\text{-}Cl \quad (3.20)$$

$$Pd \cdot H + Pd \cdots Cl \cdots CH_2\text{-}CH_2\text{-}Cl \rightarrow ClCH2\text{-}CH_3 + Cl^- + 2Pd \quad (3.21)$$

$$Pd \cdot H + Pd \cdots Cl \cdots CH_2\text{-}CH_3 \rightarrow CH_3\text{-}CH_3 + Cl^- + 2Pd \quad (3.22)$$

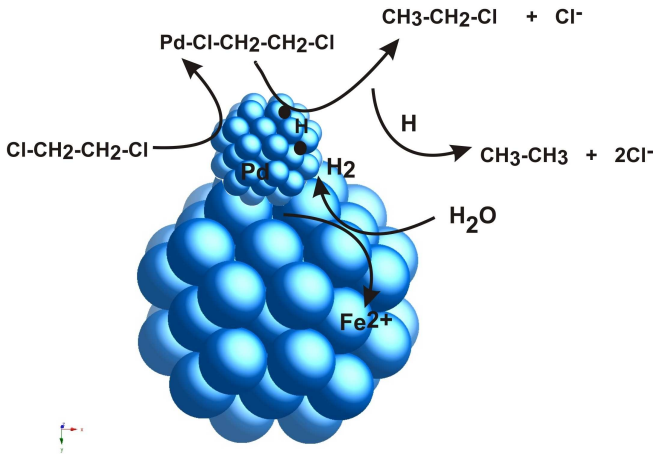

Figure 3.53 Reaction schemes for reductive transformations of 1,2 dichloroethane.

From the reaction mechanism, hydrogen formation and adsorption is an important factor in hydogrenolysis reaction. It has been proposed that atomic hydrogen adsorbed on the reductant surface (H_{ads}) is responsible for bimetal reactivity (Cook et al., 2009). However, it was also suggested that *ab*sorbed atomic hydrogen (H_{abs}) within the metal additive lattice, rather than surface-*ad*sorbed atomic hydrogen (H_{ads}), represents the reactive entity in iron-based bimetallic systems (Cook et al., 2009). in our work, better in activity of Pd/CMC-Fe^0 nanoparticles prepared by deposition of nanopalladium on the surface of Fe nanoprticles than prepared by palladization support the concept of *ab*sorbed atomic hydrogen (H_{abs}) within the Fe lattice than surface (H_{ads}). Thus, it is possible that hydrogen atoms are more solubility of atomic hydrogen in Pd noparticles rather than Pd forming an island on the surface of Fe nanoparticles.

Section III A Case Study of Using Zero-Valent Iron Nanoparticles for Groundwater Remediation

Contaminant water samples were collected from 3 groundwater wells in Map ta Phut town, Muang District, Rayong Province. Sample 1 was collected from groundwater well in Map Ya community. Sample 2 and sample 3 were collected from groundwater wells in Neon Pha Yom community and Nong Nam Yen community, respectively. The collected samples were kept in plastic bottles and stored at 4°C. The chemical and physical quality of the water such as pH, dissolved oxygen (DO) salinity and the amount of 1,2 dichloroethane contaminant in collected water samples were measured compared to the N_2 purged deionized water. The results are shown in Table 3.4.

Table 3.4 the properties of the contaminant water samples collected from groundwater wells in Map ta Phut town

Water sample	pH	DO	Salinity (ppt)	1,2 dichloroethane
1	6.34	2.48	0.614	non detectable
2	5.34	2.23	0.141	non detectable
3	5.74	1.94	0.351	non detectable
N_2 purged deionized water	5.49	3	0.014	non detectable

According to table 4.6, the pH of groundwater samples was in range 5.74-6.34 which more acidic than the groundwater quality standards (7-8.5) (ref). In addition, dissolved oxygen was also lower than the groundwater quality standards (6 mg/L). For salinity, the dissolved salt content in the water was measured by conductivity method at 25°C. The more salt that is dissolved in the water, the higher the water conducts electricity was obtained. The salinity of sample No.2 and 3 was found lower than the groundwater quality standards (0-0.5 ppt) while the sample No.1 was found higher than 0.5 ppt. These parameters can affect to the stability mobility and activity of Fe^0 nanoparticles. This work, the dispersion stability, oxidation stability, mobility and activity of Fe^0 nanoparticles dispersed in different water samples were further explored. The results are shown in Table 3.5.

Table 3.5 Stability and mobility activity of the colloidal Pd/CMC-Fe^0 nanoparticles in groundwater samples collected from different area.

Groundwater sample	[1]Dispersion stability	[2]Mobility
1	12	0.51
2	9	0.58
3	5	0.44
N_2 purged Deionized water	>30	0.30

[1] Dispersion stability was monitored by collecting the time (days) that the aqueous colloidal of Pd/ time and after adding for 7 days. The ratio of the nanoparticle to water was 2gFe/L

[2]Mobility was determined by sand column experiment, expended time for all colloidal suspension samples pass through the sand column was measured. Rate of flow (min/ 10 ML)

From table 3.5, it showed that the quality of groundwater affected to the stability and mobility of the colloidal Fe^0 nanoparticles. The ability of Fe^0 nanoparticle that remain in suspension in the colloidal form and the ability to transport to soil layers were lower than deionized water samples. These may effect to the dechlorination efficiency of Fe0 nanoparticles. In order to determine the dechlorination efficiency of Pd/CMC-Fe nanoparticles, all collected ground water samples were added with 1,2 dichloroethane and the concentration was adjusted to 5 ppm. The percentage of dechlorination is shown in Table 3.6.

Table 3.6 % dechlorination of 1,2 dichloroethane contaminant in groundwater samples

Water sample No.	% dechlorination of 1,2 dichloroethane
Sample 1	5.24
Sample 2	6.19
Sample 3	9.71
N_2 purged dionized water	13.77

%

Dechlorination of 1,2 dichloroethane was measured on the following parametres: the initial concentration of 1,2 dichloroethane was 5 ppm, the ratio of Pd/CMC-Fe nanacatalyst to solution was 2 g/1000 ml, reaction time was 24 h.

It can be seen that the dechlorination efficiency of Pd/CMC-Fe^0 nanacatalyst in groundwater is lower than in deionized water. About 50% decrease in activity was obtained. It is possible that pH, dissolved oxygen and salinity of ground water may limit the effectiveness of nanoparticles because the sorption strength and agglomeration. pH is an important factor affected to degradation efficiency of Pd/CMC-Fe^0 nanopartices. It is strongly influences the redox reactions occurring at the Fe^0 nanoparticle surface by accelerating corrosion at low pH and passivating the iron surface at high pH through the formation of ironhydroxides**.** The corrosion of Fe nanoparticles to produce H_2, which is more favored at lower solution pH; and the hydrodechlorination of 1,2 dichoroethane by H_2 (or atomic hydrogen) at the Pd surface, which is also favored at lower pH since lowering pH produces more H_2 (Wang et al., 2009).

The effect of dissolved oxygen in water is an important factor indicated the catalytic performance of Fe^0 nanocatalyst. At lower level of dissolved oxygen, the oxidation stability was clearly increased and the percentage of dechlorination was significant No. 3. Although the pH of the sample number 1 is lower but the oxygen dissolved is higher, the dechlorination efficiency of sample 3 becomes higher than sample 1.

In groundwater, there are some monovalent cations such as Na^+ and K^+ and divalent cations such as Ca^{2+} and Mg^{2+} contaminant**.** The divalent cations have greater effects on zero valent iron nanoparticles mobility than monovalent cations (Lin et al., 2010)**.** The mobility of Fe nanoparticles is generally decreased when ion concentrations increases respectively. This work, sanility and conductivity were used to monitor the effect of ionic strength to the ability of Fe^0 nanoparticles to transport in ground water. Higher conductivity and salinity of sample 1 cause an increase aggregation of Fe^0 nanoparticles resulting in decrease in rate of mobility.

CHAPTER 4

CONCLUSIONS AND SUGGESTIONS

Surface modified zero-valent iron nanoparticles were synthesized in an aqueous solution by chemical reduction method. Sodium borohydride was used as reducing agent. Different polymer stabilizers and support materials were used to investigate their ability to protect Fe^0 nanoparticles from aggregration. Sodium carboxy methyl cellulose (CMC) and water soluble starch were used as green-polymer stabilizer.

CMC stabilized zero valent iron nanoparticles were prepared at pH 8. The results from UV-visible can be used to confirm the strong interaction on CMC-Fe^{3+} complex. At this pH 8, the carboxylic groups of CMC are fully disassociated and strongly bind with Fe–O–. The stabilization mechanism of CMC-Fe^0 nanoparticles was eludicated by infrared spectroscopy technique. The sharper of peak and stretching frequencies of symmetric and a symmetric –COO- are shift to lower wavelength indicate strong interaction between Fe and hydroxyl and carboxylate group of CMC which imply to the stability of CMC-Fe^0 nanoparticles. Binding mode between CMC and Fe^0 was assigned to monodentate chelating. The soluble starch was also used as stabilizer. At pH 8, deprotonation of OH group and coordination between Fe and –CO- in starch is not occurred. Most of hydroxyl groups are in protonate form, the stability of starch-Fe nanoparticles resulted from the formation of intramolecular hydrogen bonding in starch structure. Hydroxyl groups of starch may act as the passivating contacts, thereby preventing the resultant nanoparticles from agglomeration. TEM and SEM were used to study the particle size and dispersity. The particle size of the synthesized CMC-Fe^0 nanoparticles and STR-Fe^0 nanoparticles are in range between 12-75 nm. The particles are discrete particles without chain like aggregation. Different parameters affected to the particle size of CMC-Fe^0 nanoparticles were studied such as reaction temperature, reaction time, concentration of Fe^{3+} and mole ratio of Fe^{3+} to stabilizer. The results showed that the particle size of Fe^0 nanoparticles decrease when the initial concentration of Fe^{3+} was decreased and the ratio of CMC increase. Increasing in reaction temperature, the obtained particles tend to smaller.

Zero-valent iron nanoparticles were also synthesized in the presence of support materials. Mesoporous silica nanoparticles were successfully synthesized. Monodisperse spherical particles with porous structures with the average particle size diameter 58 ±10

nm were obtained. Nanoscale zero-valent iron supported on mesoporous silica was synthesized via a wet-impregnation route followed by the chemical reduction of Fe^{3+} with $NaBH_4$. 10% of Fe loading on silica was obtained (EDX analysis) however the destruction of mesoporous structure can be noticed. Activated carbon was also used as support material. Activated carbon was pretreated with HNO_3. Infrared spectroscopic analyses of the HNO_3 treated carbons showed strong absorption of carboxylic acid groups and hydroxyl groups. Zero-valent iron Nanoparticles on activated carbon supporting (Fe^0/C nanoparticles) were prepared by chemical reduction-deposition. pH of the mixed solution Fe^{3+} and carbon was adjusted to 8. The results from TEM and SEM clearly showed Fe^0 particles deposited on carbon support. The average partilcle size of Fe^0 nanoparticles on carbon support was 75 nm.

Pd-modified Fe^0 bimetallic nanoparticles were prepared by 2 two step reaction; namely palladization and nano-palladium deposition. Pd/CMC-Fe^0 nanoparticles were use as a representative sample. For palladization, the island surface structure of the sample was proposed while nano-palladium deposition, smaller spots which darker in contrast from TEM images were assigned to the particles of Pd metals. In addition interaction between Pd and Fe atoms was proposed.

The synthesized zero-valent iron nanoparticles and Pd modified zero-valent iron nanoparticles were characterized by various techniques. The results from XRD reveal the existence of an amorphous phase of iron. The sample prepared at low temperature, a characteristic peak of zero-valent iron (α-Fe) represents bcc (body-centered cubic crystal) Fe^0 lattice planes (110) while at elevate temperature the presence of both α-Fe and iron oxide (Fe_3O_4 and γ-Fe_2O_3) crystalline phases was indicated. The results from X-ray photoelectron spectroscopy showed that the shell was mainly ferrous ion. Energy-dispersive X-ray spectroscopy (EDX) was used to study the elemental composition of Pd/Fe bimetallic nanoparticles. The results showed some variation between the value of the element contents obtained from calculated and EDX analysis. Leaching of Fe atoms due to oxidation reaction and washed out was proposed.

Stability and mobility of the synthesized zero-valent iron nanoparticles was preliminary test. For dispersion stability, bare iron nanoparticles settled to the bottom in less than 30 min while iron nanoparticles prepared in the presence of stabilizer or support

materials remain suspend over a longer time. The prepared CMC-stabilized zero-valent iron nanoparticles remains in suspension over an extended period of time (> 1 months) with no noticeable sedimentation or flocculation. Fe/C nanoparticles have lower dispersion stability in comparison with CMC-Fe nanoparticles. It can remain in colloidal suspension less than 15 days. The order of colloidal stability was CMC-Fe nanoparticles > Fe^0/C nanoparticles > Fe/SiO_2 nanoparticles > STR-Fe^0 nanoparticles. The oxidation stability increases in the sequence Fe^0/C > CMC-Fe^0 > Fe^0/SiO_2 > STR-Fe^0. For mobility test by sand column experiment, only the colloidal dispersion of CMC-Fe and Fe^0/C nanoparticles can fully pass through the column. Particle size and potential stability in colloidal suspension was analyzed by dynamic light scattering (DLS) and zeta (ζ) potential. The hydrodynamic size measured by DLS more than 10 times higher than TEM. For zeta potential analysis, CMC-Fe^0 and Fe^0/C nanoparticles showed more negative value than 30 mV which considered as stable colloids.CMC-Fe nanoparticles and Fe/C nanoparticles are high-ability materials to use in *in situ* remediation of contaminant groundwater.

Catalytic performance of the synthesized Fe^0 nanoparticles and Pd/Fe^0 bimetallic nanoparticles toward dechlorination of 1,2 dichloroethane contaminant in water was investigated in laboratory scale. The amount of 1,2 dichloroethane was analyzed on a Hewlett Packard HP 5890 series II gas chromatograph with FID detector. Head space–solid-phase microextraction (HS-SPME) and gas chromatography were used for the determination of 1,2 dichloroethane contaminant in water. The best extraction efficiency of 1,2 dichloroethane at 23°C was achieved at adsorption time of 7 min. The optimum volume ratio of sample to headspace was 10/10 mL. The optimum desorption time was 7 min at 23 °C.

The catalytic performance of Fe^0 nanoparticles toward dechlorination of 1,2 dichloroethane was found depend on their particle size. Decreasing the particle size of CMC-Fe^0 nanoparticles from to 45 to 12 nm, the dechlorination activity was increased from 1 to 5 percent. For Pd modified bimetallic nanoparticles, different techniques of adding Pd on The Fe^0 nanoparticles were found effect to the dechlorination efficiency. The CMC stabilized Pd/Fe^0 nanoparticles prepared by nano-palladium deposition exhibited nearly two times greater reactivity toward dechlorination of 1,2 dichloroethane than the Pd/Fe^0 nanoparticles prepared by palladization. The maximum percent dchlorination was reach to 14 at 0.2% Pd loading on Fe partices. The catalytic dechlorination of 1,2

dichloethane are consistent with their colloidal dispersion stability and oxidation stability. CMC-Fe nanoparticles with particle size 12 nm showed the highest dechlorination efficiency due to its high surface area, high dispersion stability high oxidation resistance. The main product from the reductive dechlorination of 1,2 dichloroethane was ethane which indicated that the dechlorination follows hydrogenolysis reaction.

From the study of groundwater collected from 3 communites nearby Map Ta Phut industrial estate, 1,2 dichloethane was not found contaminated in the collected water. A known quantity of 1,2 dichloroethane was added. Dechlorination efficiency of Pd/CMC-Fe^0 nanoparticles toward dechlorination of 1,2 dichloroethane was significant lower than artificial contaminant water. pH, dissolved oxygen and salinity of ground water was found limit the effectiveness of Fe nanoparticles due to less dispersion stability and oxidation stability.

Suggestions for Future Work

This research described method to develop catalytic performance of zero-valent nanoparticles by design and controlled synthesis. Here, several suggestions for further investigations are proposed. In summary, they are:

1. Density function calculations for studying the interaction at surface between different size of Fe and 1,2 dichloroethane should be study to support experimental results.
2. From the characterization, Pd/Fe/C nanoparticles will be another promising catalyst to degrade 1,2 dichloethane however, we have no results about their acitivity due to the limitation of extraction by HPME fiber. Activated carbon could not be separated out from the reaction cause the effect of salting. Other extraction techniques should be applied.
3. In laboratory testing, there are many limitations cause the condition different from the nature. The model study or a field case study on dechorintion efficiency should be performed.

REFERENCES

Alahmadi, S.(2012). Modification of Mesoporous Silica MCM-41 and its Applications: A review. *OJCHEG*, 28, 1-11.

Allabaksh, M.B., Mandal, B.K., Kesarla, M.K., Kumar, K.S., & Reddy, P.S. (2010). Preparation of Stable Zero Valent Iron Nanoparticles using Different Chelating Agents. *Journal of Chem. Pharm*, 2, 67-74.

Atkinson, R., & Arey, J. (2003). Atmospheric Degradation of Volatile Organic Compounds. *Journal of Chem*, 4605-4638.

Balani, F., Amico, N.D., Griffone, L., Santoro, M., & Talabella, C. (2006). Determination of Volatile Organic Compounds by Headspace Trap. *Journal of Chromatographic Science*,44.

Chen, K.F., Li, S., & Zhang, W.X.(2011). Renewable hydrogen generation by bimetallic zero valent iron nanoparticles. *Journal of Chemical Engineering* ,170, 562–567.

Cirtiu, C.M., Raychoudhury, T., Ghoshal, S., & Moores, A. (2011). Systematic comparison of the size, surface characteristics and colloidal stability of zero valent iron nanoparticles pre- and post-grafted with common polymers. *Colloids and Surfaces A: Physicochem*, 390, 95– 104.

Cook, S.M. (2009). Assessing the Use and Application of Zero-Valent Iron Nanoparticle Technology for Remediation at Contaminated Sites. 2009.

He, F. (2007). Preparation, characterization, and applications of polysaccharide-stabilized metal nanoparticles for remediation of chlorinated solvent in soil and groundwater. Auburn, Alabama, 2007.

Huang, C.C., Lo, S.L., Tsai, S.M., & Lien, H.L. (2011). Catalytic hydrodechlorination of 1,2-dichloroethane using copper nanoparticles under reduction conditions of sodium borohydride. *Journal of Environmental Monitoring*, 13, 2406-12.

Hwang, Y.H., Kim, D.G., & Shin, H.S., (2011). Effects of synthesis conditions on the characteristics and reactivity of nano scale zero valent iron. *Applied Catalysis B: Environmental*, 105, 144–150.

Innovatech Labs for more information. (2014). Headspace analysis. Retrieved January 12, 2014, from innovatechlabs.com/analytical-services-gcms-headspace-analysis.htm.

Jamei, M.R., Khosravi, M.R., & Anvaripour. (2014). A novel ultrasound assisted method in synthesis of NZVI particles. *Ultrasonics Sonochemistry*, 21, 226–233.

Jiemvarangkul, P., Zhang, W.X., & Lien, H.L. (2011). Enhanced transport of polyelectrolyte stabilized nanoscale zero-valent iron (nZVI) in porous media. *Journal of chemical engineering*, 170, 482-491.

Johnson, R.L., Johnson, G.B., Nurmi, J.T., & Tratnyek, P.G. (2009). Natural Organic Matter Enhanced Mobility of Nano Zerovalent Iron. *Environ. Sci. Technol*, 43, 5455–5460.

Joo, S.H. (2006). Nanotechnology for environmental remediation. Spinger science, USA.

Ling, X.F., Li, J.S., Zhu, W., Zhu, Y.Y., Sun, X., Shen, J., Han W.Q., & Wang, L.J. (2012). Synthesis of nanoscale zero-valent iron/ordered